Universidade de Aveiro Departamento de Ciências Médicas
2019

DANIEL MARCOS DA SILVA RESENDE

Impacto do stress do RE e sua reversão por chaperonas químicas, em vias associadas ao envelhecimento e proteostase

Impact of ER stress and its reversion via chemical chaperones, on age- and proteostasis-associated pathways

Universidade de Aveiro Departamento de Ciências Médicas
2019

DANIEL MARCOS DA SILVA RESENDE

Impacto do stress do RE e sua reversão por chaperonas químicas, em vias associadas ao envelhecimento e proteostase

Impact of ER stress and its reversion via chemical chaperones, on age- and proteostasis-associated pathways

Dissertação apresentada à Universidade de Aveiro para cumprimento dos requisitos necessários à obtenção do grau de Mestre em Biomedicina Molecular, realizada sob a orientação científica da Professora Doutora Sandra Isabel Moreira Pinto Vieira, professora auxiliar convidada do Departamento de Ciências Médicas da Universidade de Aveiro e coorientação do Professor Doutor Fernando Manuel Tavares da Silva Ribeiro, professor adjunto da Escola Superior de Saúde da Universidade de Aveiro

Este trabalho contou com o apoio da Fundação para a Ciência e a Tecnologia, pelo POCI/COMPETE2020, POR centro (Centro2020), POR Lisboa (Lisboa2020), POR Algarve (CRESC Algarve 2020), via projeto pAGE - Protein aggregation across the lifespan (CENTRO-01-0145-FEDER-000003), Instituto de Biomedicina (iBiMED) (UID/BIM/04501/2013; UID/BIM/04501/2019), e da Unidade LiM de microscopia, um nó da Plataforma Portuguesa de Bioimagem (PPBI-POCI-01-0145-FEDER-02212).

Dedico esta dissertação à minha família, o alicerce da minha vida,.

o júri / the jury

presidente / president

Professor Ramiro Daniel Carvalho de Almeida
Professor Auxiliar do Departamento de Ciências Médicas da Universidade de Aveiro

vogais / examiners committee

Professora Doutora Raquel Monteiro Marques da Silva
Investigadora Auxiliar da Universidade Católica Portuguesa, Faculdade de Medicina Dentária
(Arguente Principal)

Professora Doutora Sandra Isabel Moreira Pinto Vieira
Professora Auxiliar Convidada do Departamento de Ciências Médicas da Universidade de Aveiro
(Orientadora)

agradecimentos / acknowledgements

A primeira palavra será naturalmente para os orientadores que me acompanharam ao longo deste ano de dissertação. À Doutora Sandra Vieira, um obrigado pelo acompanhamento, boa disposição e à vontade que tornaram esta jornada mais prazerosa. Ao Professor Fernando Ribeiro, bem como à sua equipa, por toda a ajuda indispensável para a realização desta prova.

A toda a equipa sob orientação da Doutora Sandra Vieira, o meu muito obrigado. À Bárbara, por toda a ajuda fulcral em todos as fases da minha jornada e por ter funcionado como uma figura maternal nesta aventura. À Raquel, pela orientação e simpatia, bem como a capacidade de transmitir um ambiente "caseiro" e agradavelmente familiar. À Roberta, por todas os momentos de trabalho bem como os de risada e boa disposição. À Patrícia, agradeço pela orientação e conselhos que muito ajudaram também na realização deste trabalho.

À Filipa, à Carolina, ao Pedro e à Idália. Obrigada pela amizade verdadeira, por todos os momentos de boa disposição. Obrigado por estarem lá no meu melhor e no meu pior e de me guiarem da forma que só vocês conseguem. Obrigado por me darem o prazer de dizer que sou vosso amigo e que, independentemente da vida de cada um, recordemos com saudade estes momentos e esta jornada.

À Patrícia, minha cúmplice, um muito obrigado não chega para descrever toda a ajuda, apoio e aconselhamento que me deste ao longo deste ano de dissertação. Sem a tua calma e acompanhamento, esta jornada teria sido muito mais difícil em termos psicológicos. És a melhor parte de mim e só te tenho a agradecer pelo que me proporcionaste.

À minha família, meu pai, mãe, irmão e avós, o meu muito obrigado é insuficiente para tudo o que me deram. Vocês são a razão pela qual eu alcancei o que tenho até hoje. Obrigada pelos valores, princípios e acima de tudo boas memórias que me proporcionaram e irão continuar a proporcionar com certeza, pois vocês são a base da minha vida, indispensável.

palavras-chave

Stress do RE; Proteostase; Resposta a proteínas mal enoveladas; Autofagia; Envelhecimento; PERK; IRE1; ATF6; BAG3; ATF4; pERK1/2; Calreticulina; GRP78

Resumo

O envelhecimento permanece até hoje uma das áreas biológicas por resolver de maior importância. Muitas doenças associadas ao envelhecimento estão a aumentar de forma global. Uma característica principal associada ao envelhecimento é a proteostase, cujos diferentes componentes ainda não foram totalmente descritos em diferentes linhas celulares. Aqui, usando um modelo celular neuronal como as células SH-SY5Y, diversos biomarcadores de stress do retículo endoplasmático e de agregação proteica foram avaliados em ambientes de stress do RE induzidos por tunicamicina ou tapsigargina, bem como a sua reversão. A inclusão de agentes protetores (TUDCA) e reversores químicos da agregação proteica (compostos HA) foram incluídos para melhor avaliar essa mesma reversão do stress do RE. BAG3, ATF4, calreticulina e pERK1/2 foram algumas das proteínas incluídas nesta dissertação e a avaliação do stress do RE foi alcançada pela análise dos seus níveis de expressão proteicos e/ou génicos. A indução do stress do RE foi alcançada eficazmente tanto para a tapsigargina como para a tunicamicina, em todas as proteínas-alvo, nesta linha celular. ATF4, calreticulina e pERK1/2 foram diminuídas pela ação dos agentes protetores e, consequentemente, diminuiu o stress do RE. No entanto, para a GRP78 e BAG3, não se obtiveram resultados de reversão do stress do RE. XBP1s apenas alcançou resultados significativos de reversão no caso das condições tratadas com tunicamicina. Em suma, o stress do RE induzido por TG ou TUN foram revertidos parcialmente ou na sua totalidade com sucesso pelos agentes protetores nesta linha celular.

Keywords ER Stress; Proteostasis; Unfolded Protein Response; Aging; PERK; IRE1; ATF6; BAG3; ATF4; ERK; Calreticulin; GRP78

Abstract

Aging remains to this day one of the unresolved biology areas of upmost importance and many age-related diseases are on the rise worldwide. One of aging major hallmarks, proteostasis, has several associated pathways across different segments which have not yet been fully detailed in various cell lines and are needed to better understand the underlying aging problem. Here, using a neuronal-like cell line such as SH-SY5Y, several ER stress biomarkers and proteostasis associated targets are evaluated under ER stress-induced environment through tunicamycin (TUN) or thapsigargin (TG) presence. The inclusion of neuroprotective agents such as TUDCA and homegrown compounds (HA compounds) were also included to better evaluate successful chemical reversion of ER stress and protein aggregation through target proteins. BAG3, ATF4, Calreticulin and pERK1/2 were some of the proteins included in this report as biomarkers for ER stress induction using protein or gene expression level analysis. ER stress was effectively induced with thapsigargin or tunicamycin across all target proteins. ATF4, calreticulin and pERK1/2 protein and/or gene expression values decreased after neuroprotective agents' treatment. However, no ER stress reversion was achieved for GRP78 and BAG3. XBP1s achieved positive results only for tunicamycin-treated conditions. Overall, ER stress induction was partially or totally reverted with success by TUDCA and HA compounds in SH-SY5Y.

Contents

Figure Index

Table Index

Abbreviations

A	Ampere
ALP	alkaline phosphatase
ATCC	American Type Culture Collection
ATF4	Activating transcription factor 6
ATF6	Activating transcription factor 4
ATP	Adenosine triphosphate
BAG1/3	Bcl2-associated athanogene 1/3
BCA	bicinchoninic acid
BSA	bovine serum albumin
CHOP	CCAAT-enhancer-binding protein homologous protein
CMA	Chaperone-mediated autophagy
DAPI	4′,6-diamidino-2-phenylindole
E1/E2/E3	Enzyme 1/2/3
EGF	epidermal growth factor
EGFR	epidermal growth factor receptor
ER	Endoplasmic reticulum
ERAD	Endoplasmic-reticulum-associated protein degradation

ERK1/2	extracellular signal–regulated kinases ½
GADD34	Growth arrest and DNA damage-inducible protein 34
GRP78	78-kDa glucose-regulated protein
Hsc70	Heat shock complex 70
HSP70	Heat shock protein 70
IRE1	inositol-requiring enzyme 1α/β
LAMP2	Lysosome-associated membrane protein 2
MEM	Minimum Essential Medium
mTOR	mammalian target of rapamycin
ON	Overnight
PAS	pre-autophagosomal site
PBS	phosphate-buffered saline
PCNA	proliferating cell nuclear antigen
PERK	protein kinase RNA (PKR)-like ER kinase
PTMs	Post translational modifications
RT	Room temperature
RT-qPCR	Real-Time Quantitative Polymerase Chain Reaction
SDS	sodium dodecyl sulphate
SERCA	sarco-endoplasmic reticulum Ca^{2+} ATPase
TG	Thapsigargin
TRIC1	tailless complex polypeptide-1 [TCP-1] ring complex
TUDCA	tauroursodeoxycholic acid
TUN	Tunicamycin

UBD	Ubiqutin-binding Domain
UPR	Unfolded Protein Response
UPS	Ubiquitin-Proteasome System
WB	Western Blot
XBP1/XBP1s	X-box-binding protein 1/ XBP1 spliced form

1 Introduction

1.1 Aging and its hallmarks

Aging remains to this day one of the unresolved biology areas of upmost importance, while also being one of the most relevant topics to modern society. It can be defined as the time-related deterioration of the physiological functions necessary for survival and fertility, leading to impaired function and increased vulnerability to death, and representing one of the major risk factors for diseases including cancer, atherosclerosis and neurodegeneration[1–3]. With this, concepts such as maximum life span and life expectancy intimately relate to the area of aging. While maximum life span is intrinsic to species, referring to the maximum number of years a member of that said species survived, life expectancy refers to the average amount of time a member of a species may live, correlating to the population rather than the species itself[1].

While aging itself constitutes a scientific area of high priority, understanding its underlying social impact and worldwide statistics helps to elucidate the importance of this phenomenon, while at the same time giving a general landscape of how aging will be more and more predominant in the future. Concerning Europe, improved survival at older ages and a low birthrate have resulted in European countries having the oldest populations in the world[4], while Portugal specifically ranks as the 5th country with the highest aging index, with values of 141 aged individuals for each 100 young people. As of 2014, Portugal had more than 20.3% of people aged 65 years or older[5]. Figure 1 below demonstrates the issue of global aging population and its rapid scaling worldwide:

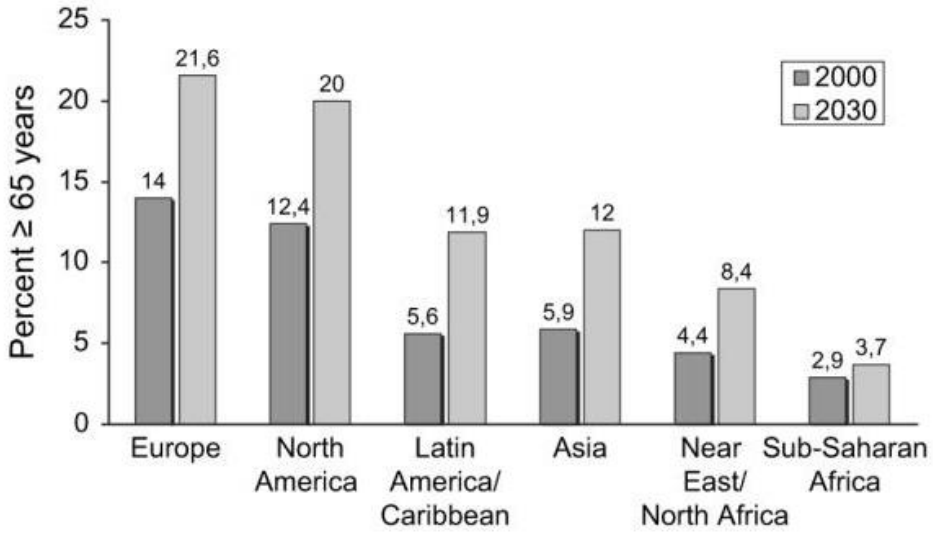

Figure 1 - Population aging throughout the world.[4]

As society grows older, age-related diseases or conditions such as hypertension, Alzheimer's disease, heart disease, cancer and stroke exponentially rise. In fact, these five leading causes of death worldwide account for 69.5% of all deaths[4]. This means that, more than ever, understanding the underlying mechanisms as well as the molecular and cellular properties associated with aging are essential to modern society development of the human body.

As in cancer research, aging has been subjected to several different models that help scrutinize and categorize the essence of this phenomenon and its underlying details, better known as hallmarks of aging. Ideally, each hallmark should satisfy the following criteria: (i) it should clearly be present during normal aging; (ii) its experimental deliberate increase should accelerate aging; and (iii) its experimental amelioration should slow normal aging process and, hence, increase healthy lifespan[3]. As of 2019, the most accepted nine hallmarks of aging are depicted in Figure 2 below:

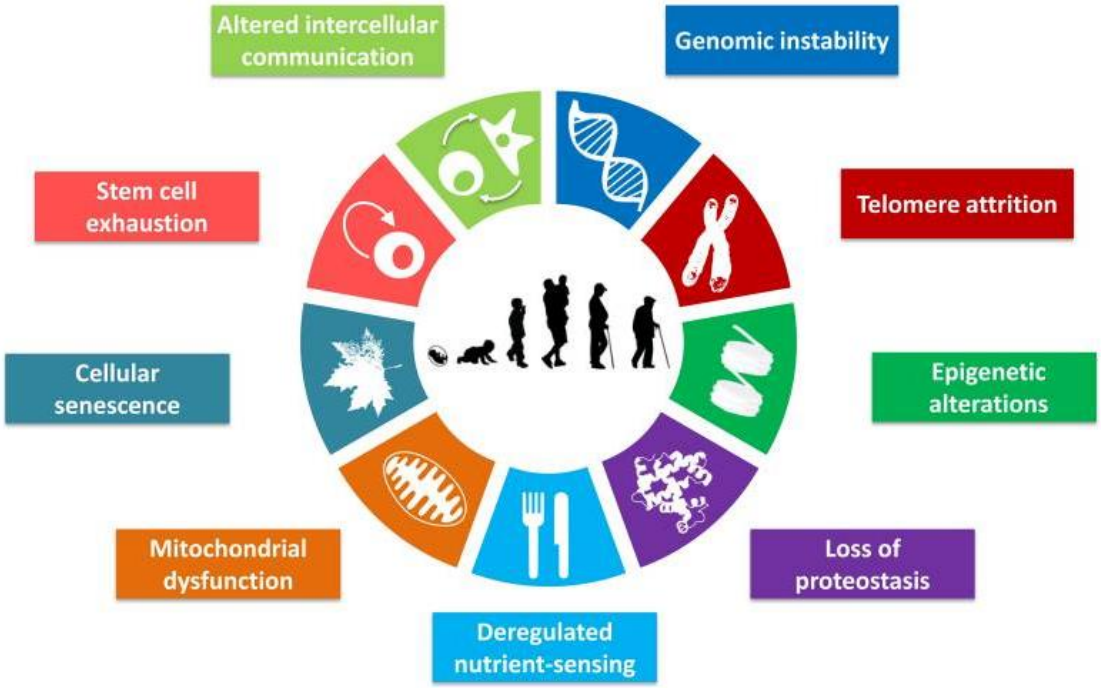

Figure 2 - Hallmarks of Aging.[3]

These nine hallmarks can be grouped into three main categories: the primary hallmarks that cause damage to cellular functions; antagonistic hallmarks in response to such cellular damage; and, finally, integrative hallmarks that are the result of a clinical phenotype[6]. However, hallmarks should not be considered definitive functions related to aging, but instead, as any group of hallmarks, should be viewed as a basic set of mechanisms that help elucidate this phenomenon.[7] This work will focus mainly in two hallmark, altered cell communication and loss of proteostasis.

1.2 Proteostasis

Proteostasis, or protein homeostasis, defines itself as the group of processes and cellular communications that regulate proteins in order to preserve both the health of the proteome and of the organism itself, resulting in a network of hundreds of biological pathways that result in a coordinated equilibrium.[8,9] It is composed by a system that acts in various subnetworks to detect and respond to protein misfolding in all cellular

compartments and regions.[10] Its high priority and importance as a scientific field of study relies heavily on the fact of it being one of the major keystones that drive the evolution of a species[11]. As a result, a complex proteostasis network in a functional equilibrium maintains a balanced proteome of the organism and, although extremely effective, it may fail, originating proteins that are folded in non-native states and therefore triggering potential cytotoxic effects on the cells.[9,11] Loss of protein structure can arise from alterations in diverse stages during protein synthesis, during the degradation process, or due to changes in concentration of metabolites in the cell environment, and is one of the major alarm triggers for the activation of the protein regulation machinery.[11]

The proteostasis network is comprised by different highly conserved sub pathways across evolution and regulated by major pathways and regulatory proteins.[11,12] The main intervenients of this network include chaperones and foldases, the ubiquitin–proteasome system (UPS), autophagy and its subtypes, the heat-shock response, the endoplasmic reticulum (ER) unfolded protein response (UPR), the integrated stress response, the ER-associated degradation machinery (ERAD), the mitochondrial UPR, and the mechanisms controlling redox balance[12]. Figure 3 shows the correlation between the major components of the proteostasis network and aging.

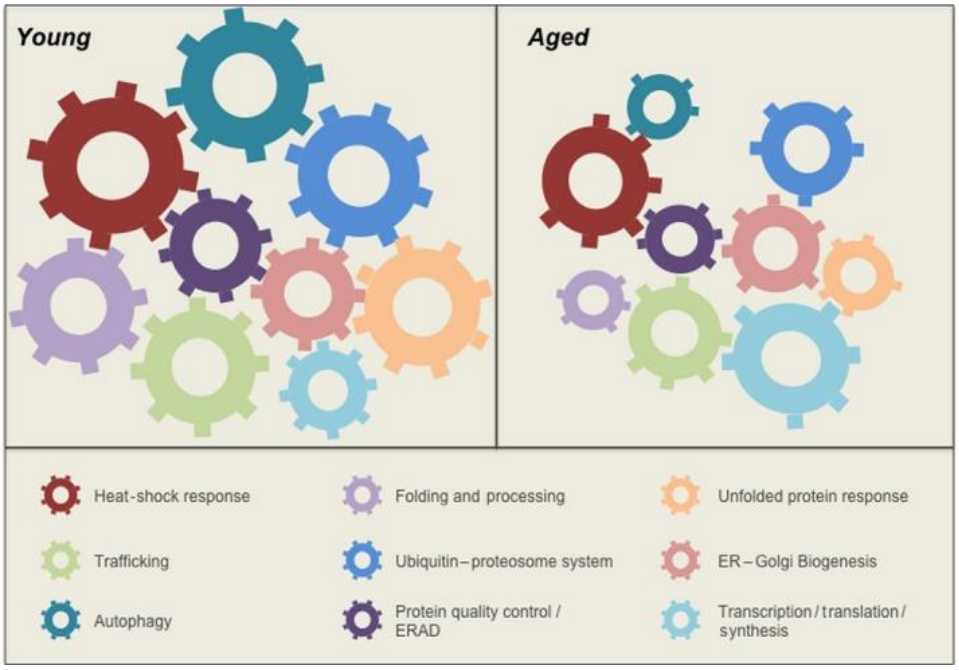

Figure 3 - The buffering capacity of the proteostasis network decreases with aging.[12]

1.2.1 The Ubiquitin–Proteasome System (UPS)

The ubiquitin-proteasome system is generally defined as a selective proteolytic system in which the conjugation of ubiquitin to substrates induces degradation by the auxiliary proteasome.[13] The proteasome is a dynamic multi-protein complex that exists in several forms. The central part of the proteasome is a 20S core particle, with a barrel-shaped structure formed by four stacked heteroheptameric rings. Two inner β-rings have proteolytic activity, and two outer α-rings form a gated pore at both ends of the barrel. Regulatory or activating protein complexes can bind at both ends of the core particle barrel to tune its activity.[14] 20S particle activity is subsequently modulated by a number of regulatory subunits including the 11S (PA28) and 19S (PA700) subunits. Interaction of the 19S regulator with the two α-rings on the 20S core, leads to the formation of a larger 26S proteasome complex that accounts for the majority of the proteolytic activity within cells[15].

Protein substrates are tagged for degradation by the covalent attachment of ubiquitin, a small evolutionarily conserved protein. This requires the coordinated action of three enzymes, hierarchically. An E1 enzyme composed of 76 amino acid must first activate ubiquitin, in an ATP-dependent manner. It forms a covalent bond between the C-terminal

end of ubiquitin and a cysteine residue in its active site, consequently transferring it to the ubiquitin-conjugating E2 enzyme. This E2 enzyme cooperates with the E3 ubiquitin ligase to transfer ubiquitin to the substrate protein, usually to lysine residues. The E3 ubiquitin ligase binds to both the E2-bound ubiquitin and the protein substrate, promoting the transfer of ubiquitin onto the substrate (Figure 4).[14,16] E3 proteins form a very diverse group. The human genome encodes 600–1000 different E3s. Such a large group of E3 proteins is required because they provide specificity for substrate selection, as opposed to the two E1 family members necessary to tag all 40 E2s with ubiquitin, in a mammalian classic UPS cascade.[16]

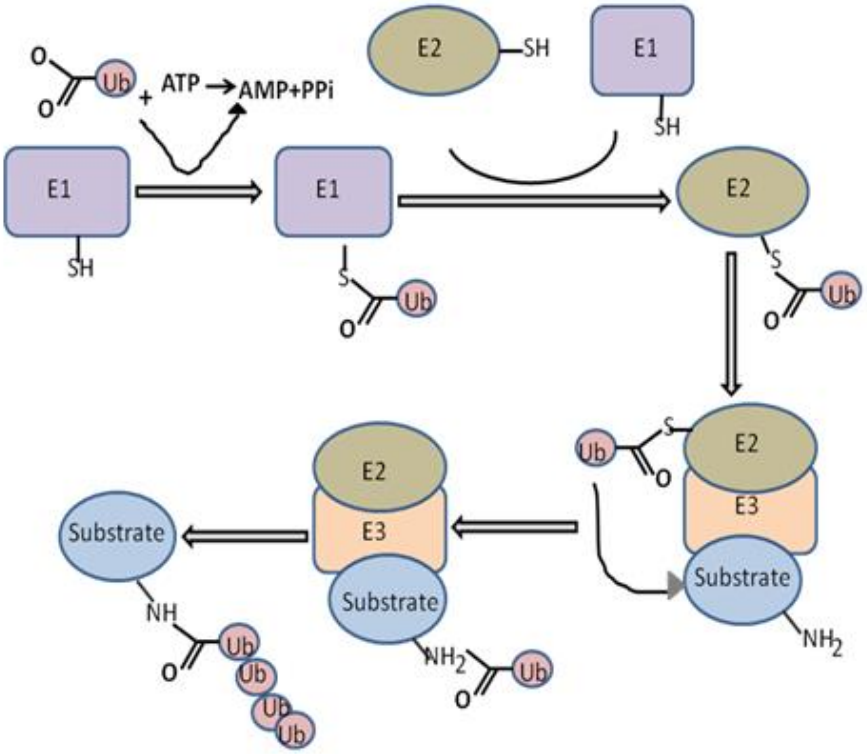

Figure 4 - Schematic of the mammalian E1-E2-E3 cascade.[16]

UPS depends heavily on the type of ubiquitination, central to the ubiquitin code, which in turn produces ubiquitin-based degrons that are recognized and bound by a class of ubiquitin-binding domains (UBDs) of specific adaptors.[13,14] Several types of ubiquitination exist (Figure 5) and they all determine the pathway through which the substrate will be degraded or transported.

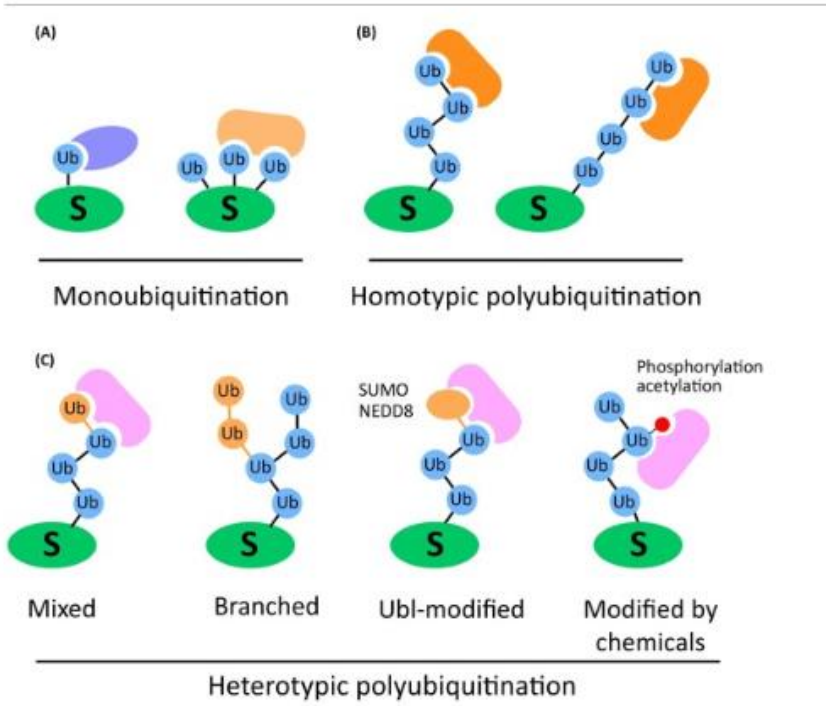

Figure 5 - Types of Ubiquitination.[13]

The ubiquitin-proteasome system, either through its proteasome activity or through the E1-E2-E3 cascade component, has been correlated to lifespan, aging and aging-related diseases, being found up or downregulated[15]. Elevated UPS activity is reported to be closely related with longevity in model organisms.[17,18] In contrast, impairing the UPS shortens lifespan in flies[19] and mice[20].

With this, all the above-mentioned criteria for an ideal aging hallmark are covered, making this regulatory system an important marker in the aging area. However, there is still a clear absence of information regarding whether there is a common underlying mechanism driving these longevity phenotypes across different mutants and models.[15]

1.2.2 Autophagy types and associated pathways

Another type of proteostatic mechanism is autophagy. Autophagy is defined as the major intracellular degradation system and stress-response catabolic process, designed to destroy and recycle unnecessary or damaged components, through their delivery to and respective degradation in the lysosome.[21,22] In contrast to the UPS pathway, it does not require the ubiquitination of the substrate. Autophagy is present at a basal level in all

mammals and is regulated by some conditions such as hypoxia, starvation or oxidative stress.[22] This catabolic process can be further categorized in three types: microautophagy, macroautophagy and chaperone-mediated autophagy (CMA), with macroautophagy being the prevalent form and the most studied one, being commonly referred simply as autophagy.[23] In terms of molecular regulation, autophagy is negatively regulated by the mTOR pathway, a signalling cascade highly associated to aging, as well by Atg proteins.[22] While the ubiquitin–proteasome system targets short-lived or oddly folded proteins, the lysosome–autophagy system targets long-lived macromolecular complexes and organelles.[24] While these 3 subtypes are morphologically distinct, they all culminate in the delivery of cargo to the lysosome. Below, Figure 6 briefly elucidates all 3 autophagy types:

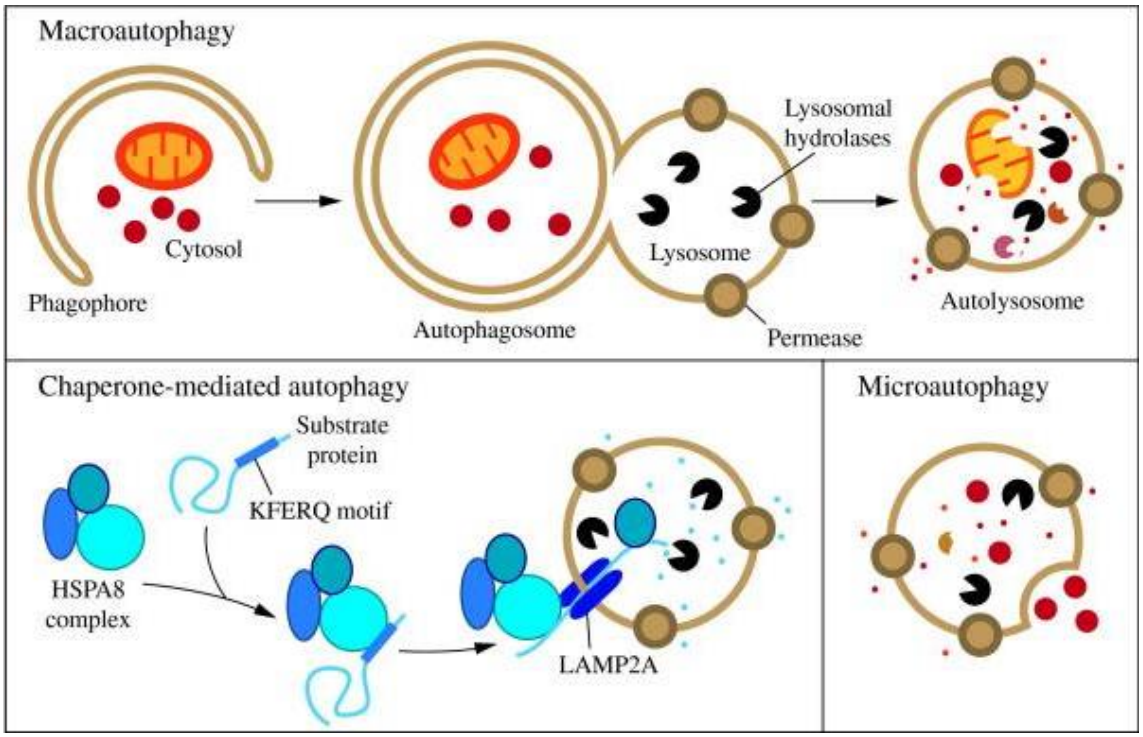

Figure 6 - Three types of autophagy.[25]

Regarding macroautophagy, the morphological hallmark of this subtype is the formation of the phagophore at the pre-autophagosomal site (PAS), leading to the formation, expansion and maturation of the autophagosome, a large cytoplasmic double-membrane vesicle. Once completely functional, the outer membrane fuses with the lysosome/vacuole, revealing the inner membrane and its cargo to nearby hydrolases.[22,26]

Figure 7 elucidates the main stages of the classic macroautophagy process. Several studies demonstrated the intricate relation between autophagy and aging, by determining that lifespan could be prolonged by stimulating autophagy through exogenous spermidine[27] and resveratrol[28], two important polyamines, in nematodes, yeast, flies and worms.

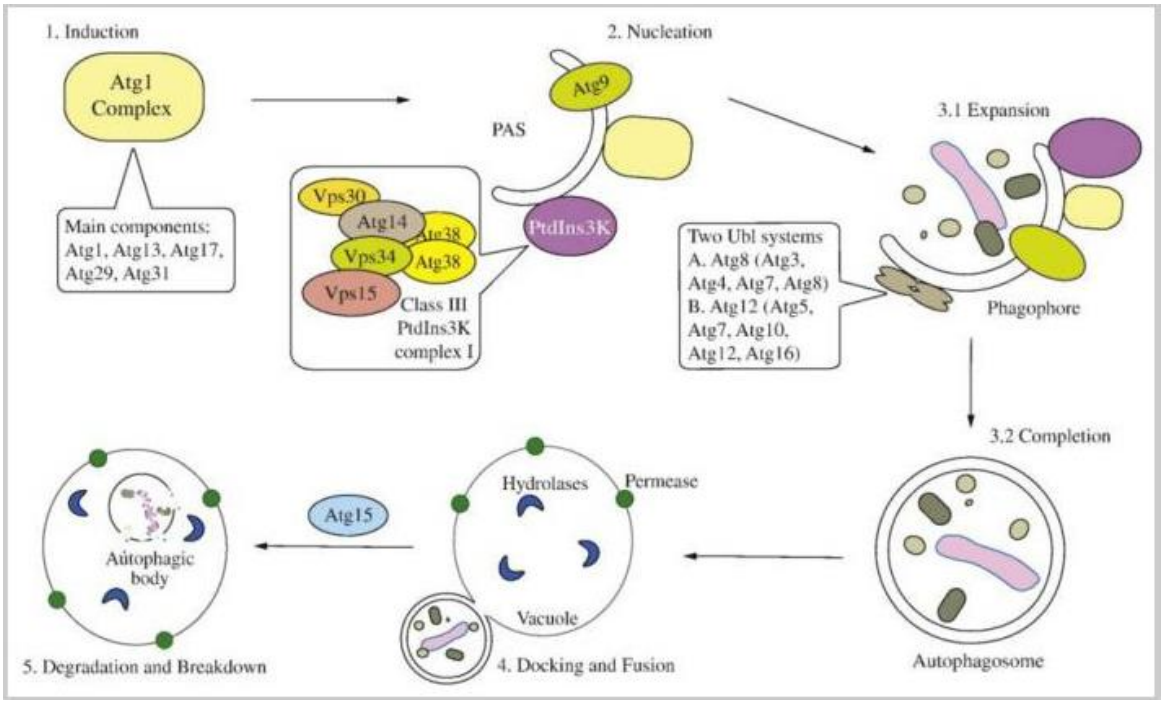

Figure 7 - Different stages of autophagy.[26]

Endosomal microautophagy is the least studied subtype. Being a non-selective lysosomal degradative process, microautophagy involves the direct engulfment of cytoplasmic cargo at a borderline membrane by autophagic tubes, which mediate both invagination and vesicle fragmentation into the lumen.[24] Little is known about the correlation between microautophagy specifically and aging, however, a report was published[29], relating the relation between impaired microautophagy through lysosomal degradation and the upregulation of ER stress and inflammation in aging adipose tissue.

The third and final type of autophagy is chaperone-mediated autophagy, similar to other types of autophagy, with the difference being how cargo delivery occurs at the lysosomes, as it does not require the formation of vesicles. Instead, the substrate proteins for this autophagic pathway cross the lysosomal membrane through a protein-translocation

complex.[30,31] With this unique property, only proteins can be targeted to this specific chaperone-mediated autophagy. Figure 8 illustrates this CMA process in three main steps: recognition; binding and unfolding; translocation and degradation.

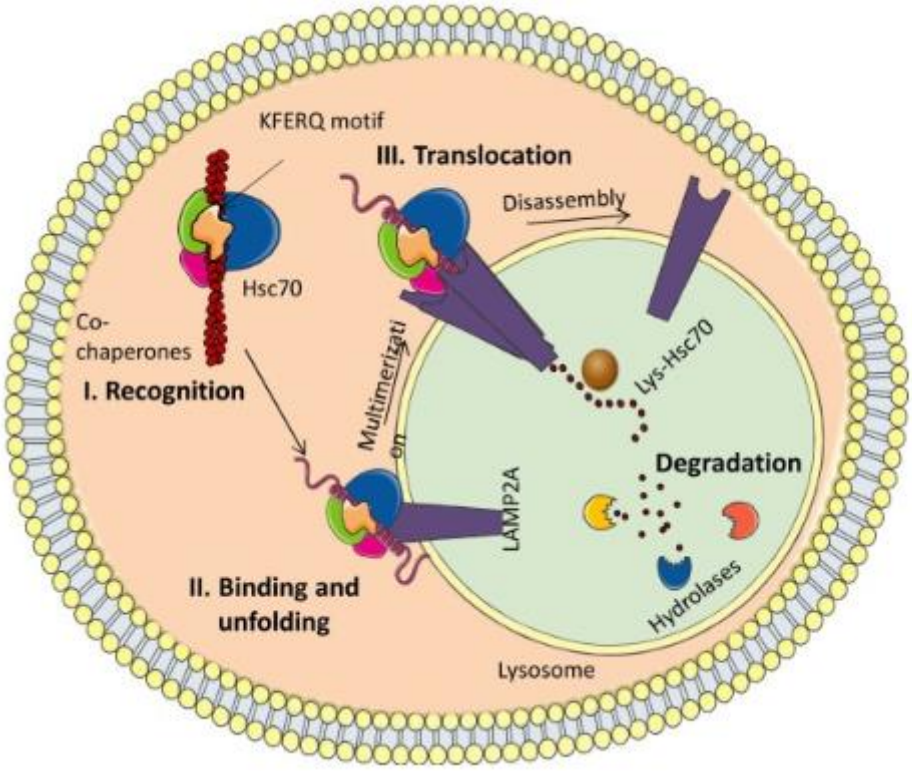

Figure 8 - Core machinery of CMA.[31]

In the recognition phase, each protein targeted for degradation by CMA contains in its amino acid sequence a specific pentapeptide motif known as KFERQ, and while the specific sequence can vary, its physicochemical properties are the same.[31] Once recognized by Hsc70, a heat shock protein, this motif and targeted protein will be carried by co-chaperones and heat shock proteins to the surface of the lysosomal membrane.[30–33] Binding and unfolding phase starts after this step, where the targeted protein/Hsc70 complex bind to LAMP2A, inducing a multimerization that allows the target unfolded protein to enter the lysosomal lumen.[34] Only unfolded proteins can cross the lysosomal membrane.[35] Finally, translocation and degradation phase consists in the activity of lysosomal chaperone Hsc70, located in the lumen, of holding and pulling the targeted protein into the lumen through the

LAMP2 complex, leading to the internalization of the protein complex, and consequently leading to its degradation through the action of lysosomal enzymes.[31] After translocation, the LAMP2A multimer is disassembled into monomers through Hsc70.[31,33]

Little is known about the underlying molecular mechanisms of how chaperone-mediated autophagy is possibly related to aging, in part because of the orchestration of this process, and because of the stochastic nature of the aging phenomena. However, several studies attempted to validate this relationship mainly using LAMP-2A as a marker for CMA activity. The first group of evidence came from young and old rat livers, where a big decrease in LAMP-2A, and therefore in the process of CMA, was observed in aged rats.[36] Other study, using early passage fibroblasts and senescent late passage fibroblasts, revealed faster degradation rates of LAMP-2A in late passage fibroblasts, under basal conditions.[37] Finally, the upregulation of LAMP-2A appears to have a beneficial effect on CMA and consequently, on lifespan. A study showed that, using transgenic LAMP-2A overexpressors in aged rat liver, CMA activity was increased, the cellular homeostasis and liver function improved as well, and there was a reduction in damaged proteins content.[38] This data clearly demonstrates a clear path towards the consensual concept that chaperone-mediated autophagy and aging are closely related.

1.2.3 Protein refolding mediated by chaperones

The third component of the proteostasis network to be illustrated is the refolding process mediated by chaperones. Almost all proteins must be folded into a defined and well characterized three-dimensional structure, that can occur multiple times throughout the lifespan of that protein.[39] Without this specific folding, proteins cannot acquire a functional activity. Severe stress inducers or environments lead to the unfolding of otherwise active proteins and consequently activate the already mentioned degradation mechanisms or, as an alternative, activate a mechanism of protein refolding that can restore the otherwise lost function of that specific protein. In other words, molecular chaperones and co-chaperones assist in the process of *de novo* folding or refolding of said protein.[40]

A broad definition of molecular chaperone is any protein that interacts with, stabilizes or helps another protein to acquire its functionally active conformation, without being

present in its final structure.[40–42] Members of these protein families are often known as the already mentioned stress proteins or heat-shock proteins (HSPs), named after the evidence that they are upregulated under conditions of stress that increases the ratio of aggregated protein. Chaperones are also usually classified according to their molecular weight.[40] Chaperones that participate broadly in *de novo* protein folding and refolding, such as the Hsp70s, Hsp90s and the chaperonins (HSP60s), are multicomponent molecular machines that promote folding through ATP- and cofactor-regulated binding and release cycles.[40–42] In short, chaperone binding to the hydrophobic regions of a non-native protein temporarily blocks aggregation, while at the same time, ATP-triggered release allows the folding to proceed.[40] Three major models illustrate the basic mechanisms of chaperone-mediated protein folding or *de novo* folding: Hsp70, chaperonin and Hsp90 models.

In the Hsp70 system, the major Hsp70 chaperones are heat shock cognate protein Hsc70 (*HspA8*) and stress-inducible Hsp70 (*HspA1A* and *HspA1B*), which are very closely related and share an ATP-dependent mechanism conserved. Other cytosolic Hsp70s are tissue-specific, or only expressed upon stress.[43–45] In short, when in an ATP-bound state, Hsp70 cannot stably bind to the substrate, while in an ADP-bound state, substrate is tightly connected to the heat shock protein. To aid in this process, co-chaperones regulate the ATPase cycle and can be divided in two classes: DNAJ co-chaperones, possessing a specific J domain that recognizes and binds to HSP70, stimulating ATP hydrolysis; and nucleotide exchange factors (NEFs), responsible for the release of ADP from Hsp70 and the consequent re-binding of ATP, to close the cycle (Figure 9).[41,43]

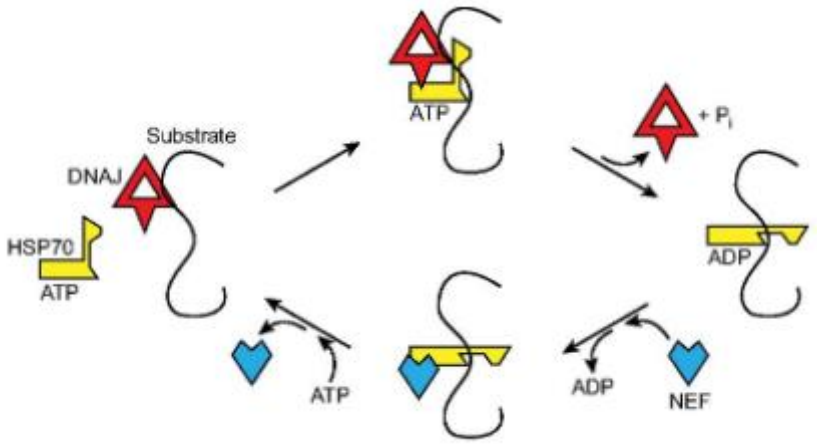

Figure 9 - HSP70 ATPase cycle.[43]

The chaperonin model is based on chaperonins, proteins whose main role is to prevent aggregation during protein folding by undergoing conformational changes that are controlled by ATP binding and hydrolysis.[46–48] These proteins can be further divided in two groups: group I chaperonins are present in the bacterial cytosol as well as the eukaryotic organelles derived from endosymbiosis; group II chaperonins are found in archaea and the eukaryotic cytosol. While group I chaperonins consists of two components, a tetradecameric Hsp60 and a heptameric co-chaperone Hsp10, group II chaperonins don't require an obligate co-chaperone, while also having two stacked rings.[46,47] Focusing on group II chaperonins, the best eukaryotic member characterized is the eukaryotic chaperonin TRiC (tailless complex polypeptide-1 [TCP-1] ring complex) or CCT (for chaperonin containing TCP-1)[47]. While little is known about the mechanisms which these chaperonins mediate folding, some efforts have been made to better elucidate this issue; based on crystal structure and other properties, this chaperonin mediates the folding of proteins who cannot be folded by other chaperone systems, like actin, while substrate itself binds to group II chaperonins through its central cavity.[49–51] Figure 10 illustrates the structural architecture of TRiC chaperonin.

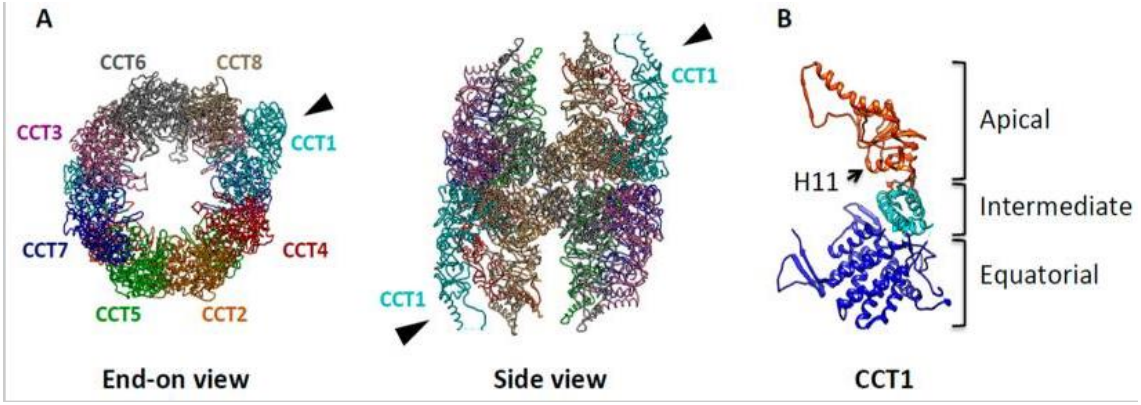

Figure 10 - Molecular structure of TRiC/CCT.[52] A) Evidently shows a double-ring structure with eight homologous but distinct subunits. B) The three domains are like the ones found in group I chaperonins and are possibly conserved.

The last major model, the Hsp90 system, relies on the properties and mechanisms of Hsp90s, a family of molecular chaperones found in bacteria and eukaryotes, but still not reported in archaea.[53] The most important Hsp90 isoforms include Hsp90α, Hsp90β, TRAP1, and GRP94 that share a common three domain organization whose function, through its N-terminal ATPase domain, is to mediate the association between the chaperone and its client proteins.[54,55] The C-terminal domain is responsible for the dimerization of the protein with the third and final middle domain. Rather than being involved in protein folding or unfolding in a classic form like other models, Hsp90s promotes subtle changes in conformation or domain arrangements in those molecules.[53]

Perhaps the most well studied chaperone model in aging research is the HSP70 system, specifically HSC70, the archetype of this model. HSP70 has been described as a possible biomarker for lifespan, since the mechanisms where this heat shock protein participates are closely related to age-related alterations such as oxidation and inflammation.[56] J-proteins and HSC70 were also described as members of a powerful regulatory network key to protein control, stress recovery and clearance of aggregates in aging using *C.elegans* as model.[57] Finally, HSP70 was described as tissue-specific regarding its basal levels and these basal levels are related to aging, being similar between prematurely aged mice and in old mice.[58]

1.2.4 The Unfolded Protein Response (UPR)

The last component of the proteostasis network here discussed is based on endoplasmic reticulum (ER) stress, more specifically, the ER unfolded protein response (UPR), a highly conserved signalling pathway. This system is essential since a very high volume of proteins is handled directly by the ER, assuring a quality protein surveillance in this organelle.[59,60] UPR is activated in response to a loss of proteostasis and is initiated by three ER transmembrane proteins – IRE1, PERK and ATF6 – inducing a counteraction to the ER stress.[60] Stressful stimuli such as hypoxia, nutrient deprivation, increased protein oxidation and disturbance of the secretory pathway may lead to an excessive accumulation of misfolded proteins at the ER, known as ER stress.[61–64] In cases where ER stress is irreversible, UPR triggers apoptosis through different mechanisms involving the upregulation of CHOP, activation of pro-apoptotic components, and induction of oxidative stress.[65,66] In cases where ER stress is reversible, the UPR induces transcription of ER chaperones to increase the ER folding capacity, and lead to mRNA decay to decrease the load of proteins in the ER (Figure 11).

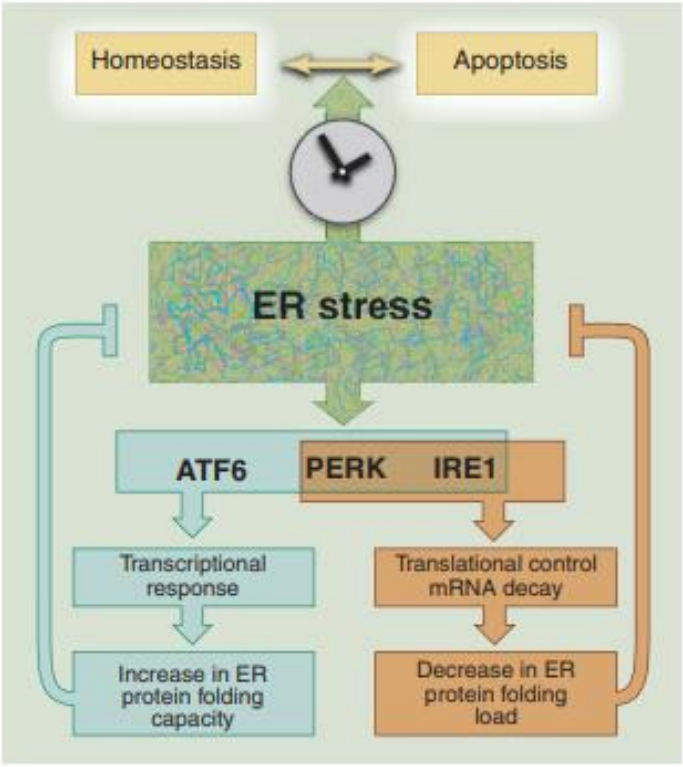

Figure 11 - UPR core elements and respective network.[60]

The activation of the ER UPR involves the presence and action of a chaperone named BiP, also known as GRP78. GRP78 consists of an N-terminal ATPase and a C-terminal substrate-binding domain and is part of the HSP70s family. In its ATP-bound form, GRP78 binds substrates with low affinity, while at the same time, those same substrates stimulate GRP78 activity to generate a higher affinity form. More, the thermodynamic hallmark of unfolded proteins - the exposure of hydrophobic regions on their surface - is recognized by GRP78. Similarly to other HSP70s, GRP78 cycles between monomeric and oligomeric states, but only its monomeric form is capable of interacting with unfolded proteins, through an ADP-ATP cycle associated with the substrate, as depicted in Figure 12.[67] In a normally functioning cell, GRP78 binds to and represses the activation of the ER stress receptors already mentioned (PERK, ATF6, and IRE1). During ER stress, GRP78 binds to unfolded/misfolded proteins and releases the ER stress receptors, promoting their activation and the induction of the UPR.[68]

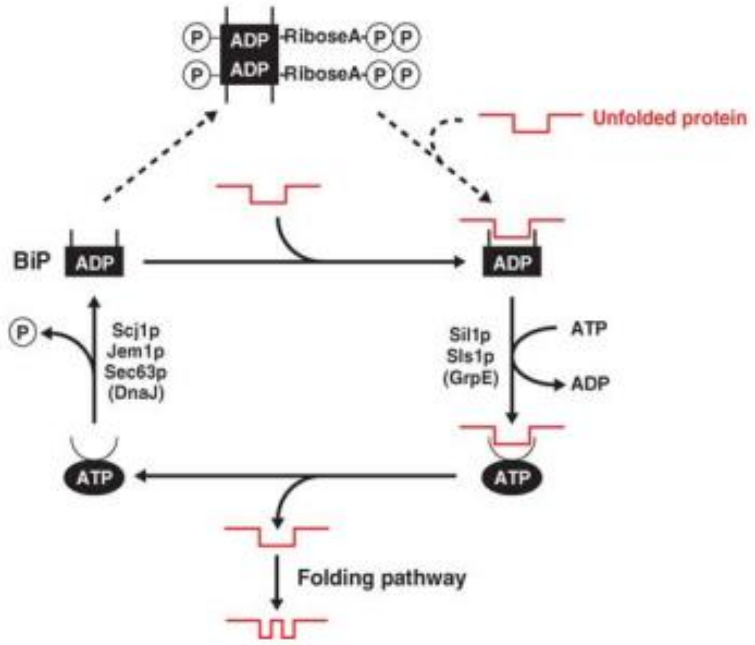

Figure 12 - BiP mode of action.[67]

ER stress and consequent UPR have been characterized in several animal models to develop the understanding of its potential relation with aging. Studies have shown that the expression of ER chaperones such as GRP78 and calnexin are downregulated in aged rats, while at the same time pro-apoptotic components such as CHOP and ER-located caspase 12 are upregulated[69,70]. Additional concurrent data from studies based on mice models, revealed that chronic ER stress might be associated with aging based on the increased levels of CHOP in aged mice when compared with young mice, after being exposed to stress-inducing agents[71]. Figure 13 illustrates the possible relation between ER stress and respective unfolded protein response and aging in well-known models.

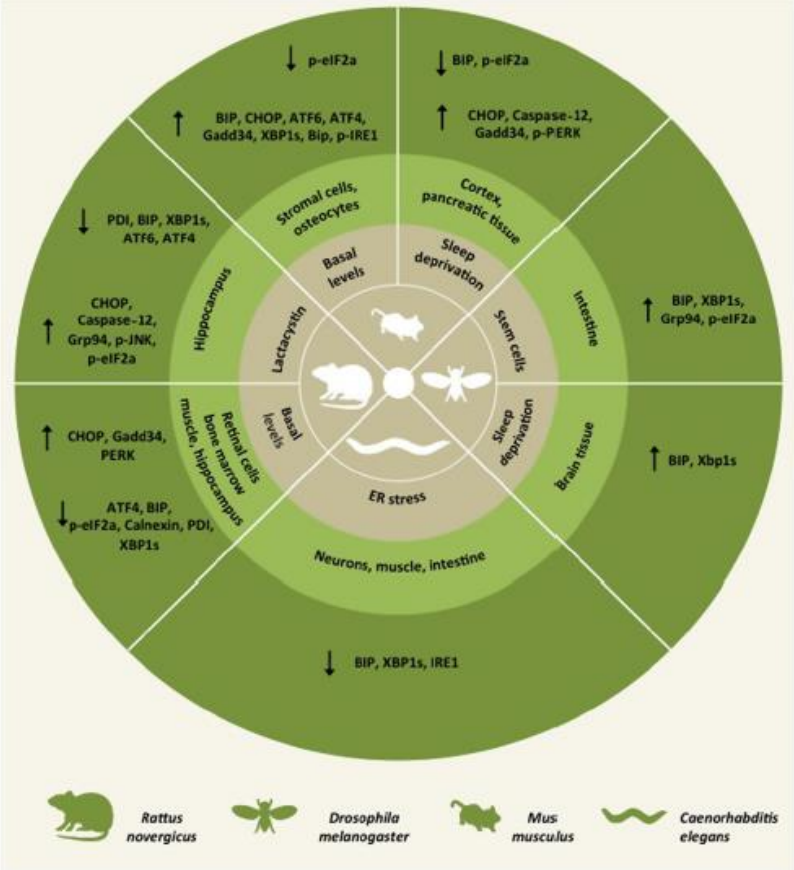

Figure 13 - Endoplasmic reticulum (ER) stress in different animal models.[12]

1.2.5. PERK/eIF2α/CHOP/ATF4 pathway

Upon activation via ER stress, PERK (protein kinase RNA (PKR)-like ER kinase) initiates an auto-phosphorylation and oligomerization process while at the same activating universal translation of initiation factor eIF2α, indirectly inactivating eIF2 and therefore, mRNA translation.[72] This initial signalling cascade helps to reduce the amount of proteins entering the ER, consequently diminishing this organelle's stress. However, some mRNAs containing short ORFs (open reading frames) in their untranslated region, such as the transcription factor ATF4, have translation priority when eIF2 is limiting, and are consequently induced.[60]

Subsequently, ATF4 induces the transcription of two target genes: CHOP (transcription factor C/EBP homologous protein) and GADD34 (growth arrest and DNA damage-inducible 34). Since the first one controls genes that are strongly involved in apoptosis, when activated at low levels, PERK branch of the UPR offers a protective environment. On the other hand, PERK pathway can be responsible for the activation of cell death pathways when highly activated. GADD34 encodes a PERK-inducible regulatory subunit of the protein phosphatase PP1C that antagonizes PERK by dephosphorylating eIF2α, contributing to the phosphorylation cycle of eIF2α and consequent activation of cell death mechanisms.[60] Figure 14 briefly illustrates the PERK branch in UPR.

1.2.6. IRE1α/XBP1 pathway

The IRE1 branch is the most conserved pathway and signalling cascade of the UPR. IRE1 (inositol-requiring enzyme 1α/β), like PERK, is activated through auto-phosphorylation and higher order oligomerization upon ER stress, through the IRE1 RNase domain.[60] IRE1α is the primary UPR mediator in mammals as it is ubiquitously expressed, whereas the expression of IRE1β is limited to mucin-producing goblet cells in the digestive tract.[73] In mammalian cells, IRE1 initiates downstream signalling through unconventional

splicing of X-box-binding protein 1 (XBP1), while at the same time it induces PTMs (post-translational modifications) via RE1-Dependent Decay (RIDD) of several substrates.[60,74]

XBP1 splicing results in the formation of a potent transcriptional activator, XBP1s, resulting in the upregulation of UPR-target genes such as ER chaperones and ERAD proteins, thus increasing the protein folding capability, while at the same time increasing protein degradation and alleviating ER stress by reducing the misfolded proteins ratio. RIDD also aids in the protein load amelioration by diminishing the load of mRNAs at the ER membrane, consequence of an endoribonuclease activity increase originated from IRE1 activation.[75] Figure 14 illustrates IRE1 branch activation and cascade.

1.2.7 ATF6 pathway

ATF6 is a type II ER-transmembrane protein with a DNA-binding domain facing the cytoplasmic side and is activated following PERK release and prior to IRE1 release from GRP78. This protein is a constitutively expressed 90 kDa transmembrane protein (p90ATF6) embedded in the ER. Contrary to PERK and IRE1, ATF6 does not undergo higher order oligomerization or autophosphorylation. Instead, this proteins translocates itself to the Golgi apparatus after GRP78 release, under a ER stress context.[68] In the Golgi apparatus, the N-terminal domain of cytosolic ATF6 is cleaved by 2 proteases, site-1 and site-2, in a process known as ‘regulated intramembrane proteolysis’. Thereafter, the fragmented section of ATF6 translocates into the nucleus and acts as a transcription factor for genes that encode ER stress response proteins, including XBP1, PERK inhibitory protein P58 and the already mentioned CHOP.[68] Figure 14 illustrates ATF6 transport and signalling cascade.

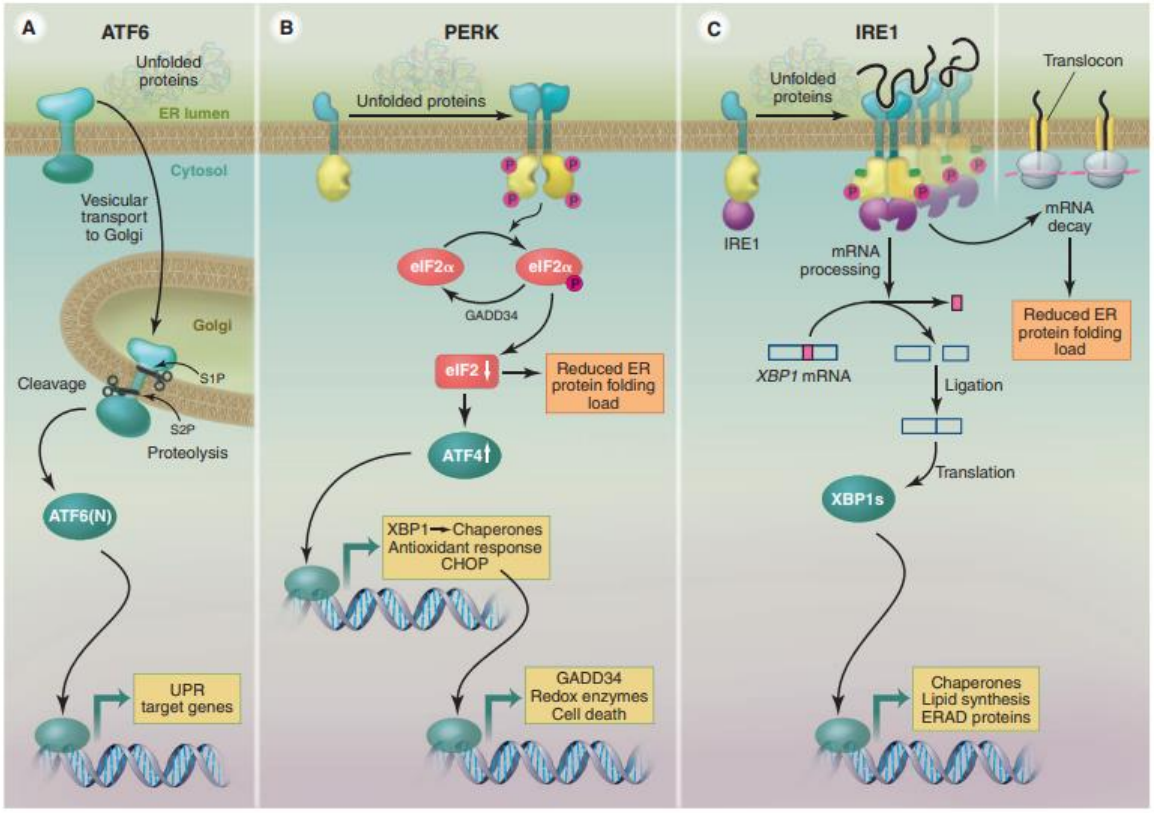

Figure 14 - Three main UPR branches: ATF6; PERK and IRE1.[68]

1.3 The ERK and BAG3 pathways in aging and proteostasis

As previously mentioned, besides altered proteostasis, imbalanced cellular signalling is another hallmark of aging, and some components of proteostasis pathways have been associated with aging. Nevertheless, this association is not fully understood.

For example, signalling pathways associated with aging, such as the EGF/EGFR/ERK pathway, are loosely associated with proteostasis. Human epidermal growth factor (EGF) is a 6 kDa protein composed of 53 amino acids. Depending on the organ, innate regulation of EGF concentrations occurs and is organ specific. EGF is implicated in the structural genesis of organs and tissues such as teeth, brain and skin.[76]. EGF binds to the EGF receptor (EGFR) and signal through the RAS-RAF-MEK-ERK MAPK pathway. The final effector ERK interacts with a large substrate spectrum to initiate various physiological and pathological responses, such as growth, proliferation, differentiation, and apoptosis

inhibition. Briefly, EGFR binds directly to GRB2 (growth factor receptor binding protein 2) and SHC (Src homology and collagen). Upon EGFR binding, GRB2 can link itself to SHC and consequently activate RAS by inducing the exchange of GDP to GTP. RAS interacts with RAF-1 that in turn, activate MEK1/2, dual-specificity kinases that activate ERK1/2. ERK1/2 is a multifunctional serine/threonine kinase that is able to phosphorylate plenty of downstream substrates which all help in the transcription and translation of Cyclin D1 and other genes, involved in proliferation, differentiation, etc..[76,77] ERK1/2 has been often related to cell longevity and lifespan through its role in cellular senescence. This kinase is an important messenger for both intracellular and extracellular signals which in turn have effects on proliferation, differentiation, cytoskeleton construction and cellular senescence[78]. However, ERK1/2 may promote senescence and not only cell proliferation in aged cells, in a cell-type dependent manner[79].

In parallel, other less studied proteostasis-related signalling molecules, such as BAG3, is being associated with aging. BAG3 is a ~75 kDa protein highly conserved in mammals and mainly localized in the cytosol, which belongs to the BAG family, a group of co-chaperones that interact with the ATPase domain of HSP70 proteins through a specific structural conserved domain (BAG domain).[80] Closely related to chaperone-mediated autophagy and chaperone protein refolding, BAG proteins are essential links between heat shock proteins and these protein regulation processes.[81] BAG3 interacts specifically with HSP70 via their conserved C-terminal BAG domain, and acts as a multifunctional protein implicated in the regulation of many processes, such as selective macroautophagy, apoptosis and cytoskeleton arrangement.[81] BAG3 has been implicated in aging-related diseases as neurodegenerations, cancer and myopathies.[81] The major relationship with aging comes from BAG3's role in selective macroautophagy and its interactions with BAG1. Both co-chaperones, BAG1 and BAG3, are reciprocally regulated during cellular aging or under acute stress. In short, BAG1 acts with HSP70 predominantly in the degradation of poly-ubiquitinated proteins by the proteasome, under physiological conditions. Under pathophysiological conditions the levels of BAG1 decrease and BAG3 increase, and BAG3 triggers the turnover of poly-ubiquitinated proteins by the autophagic-lysosomal system (Figure 15).[82,83]

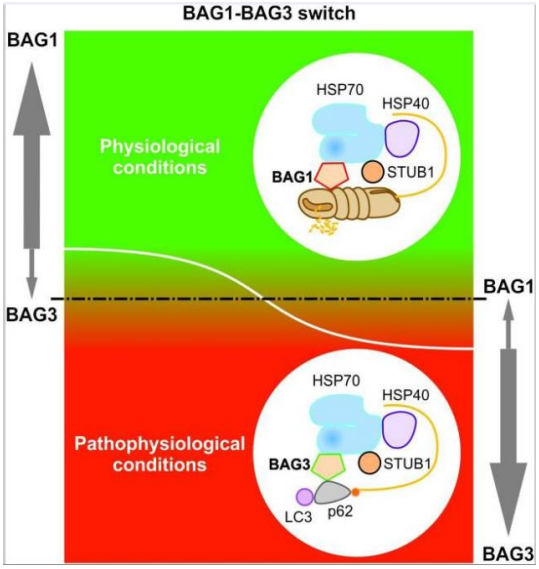

Figure 15 - BAG1-BAG3 switch in expression and function depending on cell health.[81]

In order to confirm that there were few reports in the literature relating BAG3 the EGF/ERK pathway with ER stress, particularly when induced by the well-described ER stress promoters thapsigargin and tunicamycin (see section 3.3), the literature was mined using search terms for these pathways in various cell lines. As a representative example, search terms were as follow: [BAG3] AND [thapsigargin] AND [SH-SY5Y]. Table 1 summarizes the results obtained after this literature search, for three cell lines. A relation between tunicamycin- or thapsigargin-induced ER stress (including the UPR pathways), and the chaperone-related regulator BAG3, or age-associated pathways such as ERK and other, were not well studied in several cell types, including the SH-SY5Y neuronal-like cells.

Table 1 - Literature search for studies relating ER stress inducers tunicamycin and thapsigargin and various age-associated pathways and molecules, in different cell lines.

Cell line	mTOR pathway	BAG3 pathway	EGF/EGFR/ERK pathway	PI3K/AKT pathway
Fibroblasts	TUN – 4 results TG – 2 results	No results for either TUN or TG	TG – 2 results TUN – 2 results	No results for either TUN or TG
HeLa	No results for either TUN or TG	No results for either TUN or TG	No results for either TUN or TG	No results for either TUN or TG
SH-SY5Y	TUN – No results TG- No results	No results for either TUN or TG	No results for either TUN or TG	No results for either TUN or TG

2 Aims

This report aims to better understand the relation between ER stress, induced UPR signalling pathways, and age-associated pathways such as EGF/ERK and BAG3. In order to fulfil this objective, several pathways from either unfolded protein response, aging or proteostasis groups were assayed with different methods to understand better their behaviour in specific timepoints of ER stress induction, and in the presence of protective agents that partially revert imbalanced proteostasis. More specific objectives were also established:

a. To study a relation of the unfolded protein response with the ERK pathway, which is already described to be related to aging.
b. To analyse the temporal expression profile of BAG3 in SH-SY5Y cells in the presence of ER stress inducers and ER stress protective agents.
c. To confirm the ability of in-house developed compounds to partially revert the ER stress and confirm relations between imbalanced proteostasis and age-associated pathways.

3 Materials and methods

3.1 Culture and maintenance of the SH-SY5Y cell line

SH-SY5Y, a three time subcloned neuroblastoma human cell line derived from SK-N-SH, was used for this study. SH-SY5Y cells are widely used for neuronal *in vitro* studies, due to their human origin and also due to the lack of ethical concerns associated with primary cultures. Biedler *et al*, described two morphologically distinct phenotypes in SK-N-SH cells: neuroblast-like cells (N-type) and epithelial-like cells (S-type).[84,85] Subclone SH-SY5Y also presents these distinct phenotypes[86] and can be differentiated[84] into a more neuronal-like phenotype, confirmed by the presence of neuronal markers. Undifferentiated SH-SY5Y have a neuroblast-like morphology with non-polarized cell bodies, tend to grow in clusters and proliferate continuously. Also, undifferentiated SH-SY5Y express immature neuronal markers, lack mature ones[87] and resemble immature catecholaminergic neurons, expressing proliferation markers such as proliferating cell nuclear antigen (PCNA) and differentiation-inhibiting transcription factors like ID1, ID2 and ID3[84].

Human SH-SY5Y neuroblastoma cells (CRL-2266, ATCC) were grown and maintained at 37 ºC in an incubator with 5% CO_2 humified atmosphere, using the recommended culture medium: Minimum Essential Medium (MEM):F12 (1:1), supplemented with 1.7 $g.L^{-1}$ sodium bicarbonate ($NaHCO_3$, Sigma-Aldrich); 0.5 mM L-glutamine; 10% (v/v) Foetal Bovine Serum (FBS) and 1% (v/v) antibiotic-antimycotic solution (10,000 units.mL-1 penicillin; 10,000 μg.mL-1 streptomycin and 25 μg.mL-1 Amphotericin B) (Gibco, Invitrogen, Life Technologies, USA). Medium renewal was performed every 3 days and cellular subculture was performed using 0.05% trypsin/EDTA (Gibco, Invitrogen) whenever 90% confluence was reached.

3.2 Trypan Blue assay

A common method to asses cell viability is the Trypan Blue dye exclusion assay, based on an azo dye that is membrane impermeable. The dye is able to enter unviable cells, which have compromised membranes and binds to intracellular proteins, rendering those cells blue. This allows for a direct identification and counting of live (unstained) and dead (blue) in a given population[88], using, for example, 11 µL of 0.4% Trypan Blue (Sigma-Aldrich, Dorset, UK) added to a 100 µL aliquot of cell, corresponding in this case to a dilution factor of 1.11x. Solution is incubated at room temperature (RT) for 1 minute. To count viable cells under an inverted microscope, a haemocytometer (Neubauer improved) was used and the number of cells in the suspension was calculated for each assay or experiment, considering that a volume of 0,1 µL is housed by each 4x4 square of the Neubauer chamber. The cell count procedure was performed at the time of sub-culture prior to initial cell seeding at a defined density (detailed in section 3.3).

3.3 Chemical ER stress inducers and protective agents

Thapsigargin and tunicamycin are widely used ER stress inducers *in vitro*, whilst tauroursodeoxycholic acid (TUDCA) is a gold standard ER stress protective agent. As such, these compounds were chosen to induce and revert ER stress in cells, in combination with in-house developed chemical chaperones (HA661, HA665 and HA667), cholesterol-quinoline hybrids proven to disaggregate protein aggregates and that appear to alleviate ER stress as seen by proteomic analyses (previous work in the lab; Albuquerque H. *et al*, submitted).

Thapsigargin (TG) is a sesquiterpene lactone with ability to block the autophagosome-lysosome fusion, inducing ER stress and to block Ca^{2+} pumps in the sarcoplasmic and endoplasmic reticula, preventing cells from raising cytosolic Ca^{2+} concentrations. Hence, thapsigargin is a strong inhibitor of the sarco-endoplasmic reticulum Ca^{2+} ATPase (SERCA)[89], while also being considered a tumour promoter in mammalian cells. Tunicamycin (TUN) is a drug produced by *Streptomyces lysosuperificus*, which inhibits N-linked glycosylation by preventing core oligosaccharide addition to nascent polypeptides

and thereby blocking correct protein folding and transit through the ER[90]. Tunicamycin can also, also through the same mechanism, cause SERCA oligomer insolubility and respective ER stress induction similar to thapsigargin.

TUDCA ($C_{26}H_{45}NO_6S$; MW 499.7 $g.mol^{-1}$) is an ambiphilic bile acid and a taurine conjugate form of ursodeoxycholic acid (UDCA). Humans have vestigial traces of this taurine conjugate, but bears on the other hand, contain large amounts of this acid, hence the name. This conjugate is more hydrophilic than its counterpart (UDCA) and is widely used as an investigational drug. TUDCA has anti-apoptotic, neuroprotective and anti-inflammatory properties, being a powerful mitigator of protein aggregation[91] and ER stress[92]. TUDCA is still not approved by FDA despite being a common treatment for biliary cirrhosis and cholesterol gallstones in some countries and other evidences across several health sectors.

For *in vitro* assays, SH-SY5Y were seeded at approximately $8.5x10^4$ $cells.cm^{-2}$ (85% confluency) in tissue culture polystyrene plates (60 mm, 6-well and 12-well) and were allowed to adhere for 16-18h, upon which cells were incubated with the described compounds at the following concentrations: TG (0, 10, 50, 100, 1000 nM concentrations for resazurin dose curve; 100nM for all the other assays); TUN (0.1, 1.0, 3.0, 5.0 $\mu g.mL^{-1}$ for resazurin dose curve; 1 $\mu g.mL^{-1}$ for all other assays); TUDCA (0.10, 0.25, 0.50, 1.00 mM for resazurin dose curve detailed; 100µM for all following assays); and the cholesterol-quinoline hybrids HA661, HA665 and HA667 (50 µM in all assays; concentrations previously optimized in lab).

3.4 Resazurin-based metabolic assay

To evaluate the cellular metabolism (and cell viability, indirectly) and establish dose curves for the tested compounds, a resazurin-based assay was performed. Resazurin salt (Sigma-Aldrich, Dorset, UK) is a cell permeable redox indicator, which is transformed in the reducing environment within the cytoplasm and mitochondria of metabolic active cells. Resazurin, blue and non-fluorescent, is reduced by dehydrogenase enzymes to form the pink and highly fluorescent resorufin. The amount of resorufin can be monitored by

fluorescence or absorbance, being proportional to the number of living and metabolic active cells in the sample.[93]

Cells were incubated for 4 hours with fresh complete medium containing 10% of a resazurin stock solution [0.1 mg. mL^{-1} in sterile phosphate-buffered saline (PBS) (Thermo Fisher Scientific)]. Resorufin quantification was assessed through absorbance, measured spectrophotometrically at 570 nm and 600 nm (Infinite 200 PRO, Tecan, Switzerland). Equation 1 was used to determine cellular metabolic activity based on optical density (OD) ratio of each tested condition, of cells grown without compound incubation (positive control) and of medium with 10% resazurin (a negative control used as a blank value).

$$Viable\ cells\ (\%) = \frac{OD[test\ cells]\left(\frac{570}{600}nm\right) - OD[negative\ control]\left(\frac{570}{600}nm\right)}{OD[positive\ control]\left(\frac{570}{600}nm\right) - OD[negative\ control]\left(\frac{570}{600}nm\right)} x100 \qquad (1)$$

3.5 Fluorescence Cytochemistry

In order to visualize protein aggregation complexes a cytochemistry assay was performed using fluorescent stains.

For this assay, glass coverslips in 6-well TCPS plates were previously coated with 0.1 $mL.cm^{-2}$ of poly-L-ornithine at a working concentration of 0.1 mg. mL^{-1}, diluted in PBS. Gentle agitation was followed to ensure uniform coating of culture dish. After 5 minutes, excess solution is aspired and rinsed with tissue culture grade water three times for 5 minutes. Upon the third wash, there culture plate was incubated and allowed to dry at 37ºC for 2 hours (ON drying is optional). Coating procedure with poly-L-ornithine is necessary, since SH-SY5Y cells do not properly adhere to glass coverslips and this positively charged synthetic amino acid is specific to enhance their adhesion.

Cells were seeded onto coated coverslips (seeding density detailed in section 3.2) and upon adhesion were incubated with the ER stress inducers – TG, TUN – and MG132, this last a positive control for protein aggregation that inhibits the proteasome. TG and TUN were used at two different concentrations: 100 nM and 1000 nM for TG; 1 µg. mL^{-1} and 5 µg. mL^{-1} for TUN and 5 µM for MG132. A 24h timepoint was considered as optimal for all conditions and controls. Working solutions were previously prepared and diluted in

adequate culture medium before incubation. Following incubation time, wells were washed 3 times with PBS 1x.

All conditions were fixed in 4% formaldehyde for 20 minutes at RT and properly washed three times with PBS 1x. Paraformaldehyde is a powder of polymerized formaldehyde that by itself cannot fix cells/tissues. To be used as a tissue fixative, paraformaldehyde must be dissolved in hot water to become a formaldehyde solution and therefore capable of fixing cells or tissues. Fixation procedure with formaldehyde is necessary to preserve protein targets within tissues and cells and their respective immunoreactivity as well as cell/tissue morphology.[94]

Since protein aggregates are localized mainly intracellularly, a permeabilization process was performed. Cells were washed with Triton 0.2% in PBS for 30 minutes after fixation and washed three times with PBS 1x, always protected from light. Permeabilization is necessary to allow antibodies or molecular probes to enter the cell and detect intracellular antigens[95]. The fluorescent dye Proteostat®, that stains protein aggregates, was added after permeabilization and cells were left to rest for 30 minutes in the dark. Following dye incubation, three washes with PBS 1x and one wash with PBS-T 1x were performed and coverslips were left at 4 ºC ON in PBS-T 1x solution, covered from light.

Cells were mounted on glass slides with DAPI-containing mounting media. Since Proteostat® only localizes protein aggregates, DAPI is used to ensure correct nuclear and, therefore, cellular identification.

3.6 Cells collection and protein content quantification

To analyse protein expression at 0h, 2h, 16h and 24h of compound incubation, cellular lysates were collected from 12-well plates in 100-200 µL of 1% sodium dodecyl sulphate (SDS; NZY Tech, Portugal), sonicated on ice for 20 seconds (50-60% frequency; 0.5 cycle) and boiled at 95 ºC for 10 minutes.

Total protein content was quantified through Pierce™ BCA Protein Assay Kit (PierceBiotechnology, USA) in an aliquot of each cell lysate. This kit uses a two-

component detergent-compatible formulation for a two-step reaction: (i) the reduction of Cu^{2+} to Cu^{+} by proteins in an alkaline environment (biuret reaction), (ii) followed by the colorimetric detection of Cu^{+} ions by bicinchoninic acid (BCA).[96] The biuret reaction generates a coloured chelate complex if the peptides under test contain three or more amino acid residues. The final intense purple product is originated by the chelation of two BCA molecules with one reduced ion. The colour intensity increases with the number of cations formed and, consequently, with the number of peptides with 3 or more amino acid residues. The BCA/copper complex is water-soluble with strong absorbance at 562 nm[96] presenting absorbance values that are nearly linear with increasing protein concentrations.

Protein concentration of cell lysates were calculated with reference to standard concentrations of bovine serum albumin (BSA), prepared through a series of dilutions from a 2 mg. mL^{-1} stock solution as detailed in Table 1. Both standards and cell lysates were aliquoted onto a 96-well microplate. Biological samples were prepared in duplicate by adding 5 µL of each lysate to 20 µL of the solution used for sample collection (1% SDS) Finally, to each standard or condition, 200 µL of the working reagent (WR), a mixture of BCA reagent A and B in a 50:1 ratio were added. After incubation at 37ºC for 30 minutes of the microplate and further RT cooling, absorbance was measured at 562 nm in a microplate reader (Infinite 200 PRO, Tecan).

*Table 2 - **BSA standards used for standard curve.** Volumes from BSA stock, SDS and working reagent (WR) are also depicted. Corresponding protein mass in micrograms is also shown*

BSA Standard	BSA stock (µL)	1% SDS (µL)	Corresponding Protein mass (µg)	WR (uL)
P_0	-	25	0	200
P_1	1	24	2	200
P_2	2	23	4	200
P_3	5	20	10	200
P_4	10	15	20	200
P_5	20	5	40	200

A standard curve was obtained by plotting BSA absorbance versus BSA concentration. Total protein concentration of each sample was inferred through the obtained standard curve equation. Protein concentrations obtained through this curve are further described in the result section (section 4.2.).

3.7 Real-Time Quantitative Polymerase Chain Reaction (qRT-PCR)

To further characterize the effects of ER stress inducers and protective agents on SH-SY5Y cells, a real-time qPCR assay was performed. Gene expression levels of CHOP, calreticulin, XBP1s and GRP78/BiP, proteins associated with ER stress, were analysed.

Real-time PCR coupled with reverse transcription is a widely used PCR ramification that semi-quantifies gene expression levels. This method comprises the following steps: (i) classical RNA extraction from samples, followed by (ii) reverse transcription of RNA into cDNA and (iii) chemical detection and quantification of PCR products, which can be probe based (specific) or non-probe based (non-specific)[97]. This assay brings numerous advantages over classical PCR protocols, since it only requires a small amount of sample for an accurate analysis, while at the same has the ability to reproduce rapid and accurate data for more than one gene/target at the same time (multiplexing).

In this report, SH-SY5Y cells were seeded in 60 mm plates and allowed to adhere for 16-18h before incubation with TG, TUN, TUDCA and HA665 (seeding density and concentrations detailed in section 3.2). Two positive controls, composed of either TG or TUN with no protective compound's treatment whatsoever, and one negative control (cells that suffer no treatment whatsoever), were included. After compound incubation for 24h, a homogenisation step was performed by adding 500 µL of NZYol (NZYTech, Portugal) directly to culture dishes for cell lysis. Lysate volume was thoroughly resuspended to ensure maximum cell disruption before collecting lysates into microtubes for storage at -80 ºC until further manipulation.

Phase separation was performed after the homogenisation step to separate total RNA from cells and DNA/protein contaminants. Homogenized samples were incubated for 5

minutes at RT before adding 100 µL of chloroform (Alfa Aesar, Thermo Fisher Scientific) to each microtube. Tubes were shaken vigorously by hand (15 times). Further, centrifugation was performed (15 minutes, 12 000 *g*¸ 4 ºC). Following centrifugation, a clear three-layer mixture was visible, composed of a lower green, phenol-chloroform phase that mainly contains protein; a white coloured interphase (containing DNA) and a colourless upper aqueous phase (containing RNA). Upper phase was transferred to new tubes without disturbing other phases.

RNA isolation was performed right after phase separation, with the addition of 250 µL of isopropanol (Acros Organics, Thermo Fisher Scientific) for an initial homogenization followed by a gentle mixture by hand. Samples were allowed to incubate for 30 minutes at RT. A second centrifugation was performed (10 minutes, 12 000 *g*, 4 ºC) and a white pellet of RNA is formed at the bottom and sides of the tube. The isopropanol supernatant is not completely discarded to ensure RNA pellet does not disrupt. One-time wash with 500 µL of ethanol 75%, diluted from ethanol 100% (Alfa Aesar, Thermo Fisher Scientific) with RNase free water with a 0,1% (v/v) of diethyl pyrocarbonate (DEPC) [Acros Organics, Thermo Fisher Scientific] was performed, followed by a new centrifugation (5 minutes, 7600 *g*, 4 ºC). A second wash with the same volume of ethanol 75% was performed after discarding all supernatant again, to ensure cleaning of possible contaminants (for example: phenol, isopropanol). This time, after washing, all supernatant was removed and let air-dry at room temperature. Finally, 30 µL of RNA storage solution (Thermo Fisher Scientific) was pre-warmed at 60ºC and added to each tube, and then kept on ice to be immediately quantified. RNA amount and respective purity were measured using Nanodrop 3300 (Isogen, Thermo Fisher Scientific) which retrieves RNA quantity values through OD values.

The amounts of RNA were normalized between all samples (0.75 µg of total RNA). In this experiment, 0.75 µg was considered optimal for sample normalization. A final mixture was prepared in new tubes according to the scheme in Table 3. Thermocycler (Thermo Fisher Scientific) was used to run NZYtech classical reverse transcription program.[98] Samples were stored at -20 ºC until qPCR was performed.

Table 3 - Volumes collected from each solution for reverse transcription procedure.

RNA sample (µL)	RNase free water (µL)	Master Mix (µL)	Enzyme (µL)	RNase (µL)	RNase free water (µL)	Final Volume (µL)
Volume equivalent to 0.75 µg (e.g. 1.6)	Volume to complete 8 µL (e.g. 6.2)	10	2	1	54	75
Both values are adjusted considering RNA normalisation and a constant 8 µL volume of mixture						

Following reverse transcription, q-PCR was performed to detect expression of four target genes: CHOP; Calreticulin; XBP1s; GRP78/BiP, the Master Mix was prepared by adding one forward and one reverse primer (previously drawn) relative to each target. (Table 4) cDNA samples were diluted in a 1:10 ratio and duplicated for each sample, with one negative control (with no cDNA). Hrtp1 was used as a housekeeping gene, and all values were compared to Hrtp1 relative quantities. In a proper PCR plate, 2.5 µL of sample plus 12,5 µL of the master mix was added to each well of the corresponding primer. For each condition, a duplicate was made. After sampling into PCR plate, a quick 2 min centrifugation at 800 g in a plate centrifuge was performed.

Table 4 - Volume values for qPCR

Forward primer (µL)	RNase free water (µL)	Reverse Primer (µL)	SYBR Green (µL)	Final Volume (µL)
1.5	2	1.5	7.5	12.5

qPCR was performed using CFX Connect Real-Time PCR Detection System (BioRad) using the following properties and run-times: an initial 2 min run at 95ºC,

followed by a 5 second run at 95ºC, a 55ºC run for 10 seconds and a 20 second run at 72ºC, before the first plate read. 39 similar cycles are performed with the same values followed by successive plate reads. Overall run ends with a 10 second 55ºC segment and a 5 second run at 95ºC after all cycles are performed. A final plate read is done and qPCR is finalized.

3.8 Immunoblot Assays

Cell lysates from each condition, mass-normalized by the BCA assay, were subjected to SDS-PAGE electrophoresis with a 5 to 20% polyacrylamide gradient [29:1 Acrylamide: Bis-Acrylamid solution (Fisher Scientific, Ottawa, Canada)]. After protein separation through electrophoresis, samples were eletrotransfered onto nitrocellulose membranes through immunoblot procedures. A dual colour protein standard (Bio-Rad) was ran in parallel to the test samples and allowed to monitor protein separation during the electrophoresis, helping in transfer quality assessment and molecular weight estimation.

Upon eletrotransfer, Ponceau S staining is performed to assess equal gel loading and protein transfer quality transferred to membrane. Ponceau S, a negative stain, binds reversibly to the positively charged amino groups of the protein and to non-polar regions in the protein. Briefly, nitrocellulose membranes were hydrated upon transfer with TBS 1x for 10 minutes, immediately stained by Ponceau S solution (Sigma Aldrich, 0.1% [w/v] in 5% acetic acid) for 5 minutes and rinsed in distilled water to allow bands to be visible in the white membrane background. Scanning was performed using ChemiDoc Imaging System (Bio-Rad) for density analysis by ImageLab Software (Bio-Rad). Membranes were washed with 1x TBS-T for 10 minutes until red staining from Ponceau S solution was totally removed, followed by immunological detection of the membranes.

Following Ponceau S staining, immunological detection assay was performed. Prior to antibody incubation, proper membrane hydration was assured with TBS 1x, followed by blocking of non-specific binding sites of primary antibodies by immersing membranes in in 5% non-fat dry milk blocking solution diluted in TBS-T 1x for 2 hours at RT, with agitation. Incubation with primary antibody was performed according to manufacturer's instructions, with incubation by gentle agitation overnight (ON) at 4ºC and 2 hours at RT. After primary incubation, membranes were three times washed with TBS-T 1x for 10

minutes each. Appropriate secondary antibody incubation was carried out, conjugated with horseradish peroxidase (HRP). This secondary antibody is expected to bind specifically to the primary. Incubation was performed with agitation for 1 hour at RT. Antibody solutions were prepared according to dilutions in Table 2. Following secondary incubation, membranes were washed again three times, 10 minutes each, with TBS-T 1x.

Enhanced chemiluminescence (ECL) detection method was performed to detect the immunologically labelled proteins in each sample. With this method, detection occurs when energy from a chemical reaction is released in the form of light. When in presence of HRP, a luminol-based substrate (Amersham ECL Select Western Blotting Detection Reagent, GE Healthcare Life Sciences) is oxidized and forms a product in its excited state that emits light as it decays to its ground state. Once the substrate is in proximity with the enzyme, a reaction with light emission occurs and, once substrate is exhausted, signal output ceases, generating in the meantime a chemiluminescence signal at 425 nm.[99] Membranes were incubated with the working mixture of the chemiluminescent detection reagent for 5 minutes at RT, followed by image acquisition using ChemiDoc Imaging System (Bio-Rad). Considering that light emitted is directly proportional to the amount of protein present in the membrane, a density analysis can be performed using ImageLab Software (Bio-Rad). After detection, membranes were washed three times with TBS-T 1x and one time with distilled water, dried up at RT and stored. Table 2 summarizes primary antibodies and respective secondary antibodies used.

Table 5 - Primary antibodies used in this work, their respective secondary antibodies, and the expected molecular weight of targeted proteins.

Target Protein	Primary antibody	Secondary antibody	Expected IB band(s)
Bag-3	Anti-Bag-3 protein mouse monoclonal antibody [Santa Cruz Biotechnology] Dilution: 1:1000 in 3% BSA/TBS-T	Horseradish Peroxidase conjugated α-mouse IgG Dilution: 1:3000 in 3% non-fat dry milk/1x TBS-T solution	Two protein bands relative to Bag-3 are expected at 80 and 90 kDa.

CREB-2 (also ATF-4)	Anti-CREB-2 mouse monoclonal antibody [Santa Cruz Biotechnology] Dilution: 1:500 in 3% BSA/TBS-T	Horseradish Peroxidase conjugated α-mouse IgG Dilution: 1:3000 in 3% non-fat dry milk/TBS-T solution	CREB-2 is expected at 40-50 kDa
GRP-78 (also BiP)	Anti-GRP-78 rat monoclonal antibody [Santa Cruz Biotechnology] Dilution: 1:1000 in 3% BSA/TBS-T	Horseradish Peroxidase conjugated α-rat IgG Dilution: 1:10000 in 3% non-fat dry milk/1x TBS-T solution	GRP-78 is expected at 78 kDa.
phospho ERK (1/2)	Anti-phospho-ERK rabbit polyclonal antibody [Cell Signaling] Dilution: 1:1000 in 3% BSA/TBS-T	Horseradish Peroxidase conjugated α-rabbit IgG Dilution: 1:3000 in 3% non-fat dry milk/1x TBS-T solution	phospho-ERK1/2 are expected as two bands at 42 and 44 kDa.
ERK (1/2)	Anti-phospho-ERK rabbit polyclonal antibody [Cell Signaling] Dilution: 1:1000 in 3% BSA/TBS-T	Horseradish Peroxidase conjugated α-rabbit IgG Dilution: 1:3000 in 3% non-fat dry milk/1x TBS-T solution	ERK1/2 are expected as two bands at 42 and 44 kDa.

3.9 Statistical analysis

Across all experiments performed in this report, raw values were compared to control levels and compared to control levels (of the first timepoint analysed in the case where more than one control sample is present). Following comparison, all values were converted to percentage or as fold increase, and averaged. Standard deviation (SD) was calculated based on average values and data was presented as mean ± SD (with exception of qPCR, n=1). Data from control versus treatment conditions were analysed using two-tailed student t-test using the GraphPad Prism software (USA) and statistical significance was evaluated. Differences positively significant are indicated in the respective figures and legends.

3.10 Summary of analyses

In this report, several biological outcomes were assessed to evaluate the impact of ER stress on specific signalling pathways related to proteostasis in neuronal-like cells such as

SH-SY5Y. Cell proliferation was assessed to analyse the impact of the drug treatment used in SH-SY5Y directly in its populations, using *wet lab* techniques such as cell counting, cell viability assays and protein synthesis quantification. Regarding ER stress and UPR marker proteins, ATF4 expression might be indicative of PERK activation and, therefore, of ER stress response. CHOP is also a suitable marker for PERK and ATF6 since its transcription is dependent on both ATF4 and ATF6. Also, ATF6 activation can be directly assessed on its protein level through monitoring of its cleaved 50 kDa product. IRE1 can also be monitored through direct mRNA levels of XPB1 splicing.[100] However, as a side note, using one single UPR marker isn't indicative on its own of ER stress, so combining several markers and techniques should prove optimal.

Relevant timepoints, based off literature and initial dosage curve and viability assays, were optimized for this report. With this, timepoints of 2 hours, 16 hours and 24 hours were chosen to be the best ones to complete the aims of this report. Every protocol performed was repeated at least 3 times (three biological replicas) with duplicates for each condition (two technical replicas) to ensure that a significant biological result was achieved for each procedure. Through *scale-down* and *scale-up* techniques and based off common cell culture numbers for cell dishes and its respective growth areas, optimal cell population for each well was calculated. For 6-well dishes and based also the maximum seeding value for SH-SY5Y, a population $8x10^5$ cells per well was considered optimal. Other cell dishes used throughout this report as well as 100mm, 60mm, 35mm plates used were plated using $8x10^5$ cells as a reference, after calculating values with the already mentioned *scale-down/scale-up* method.

Table 6 briefly summarizes all methods, timepoints and outcomes evaluated in this report.

Table 6 - Summary of all assays performed and respective timepoints and biological outcomes

Assay	Timepoints	Biological outcome
Resazurin assay	0h, 16h, 24h	Cellular viability and metabolic activity
IB assays of cell lysates (cellular protein markers)	0h, 2h, 16h, 24h	Expression and quantification of relevant cellular UPR/Proteostasis/Aging protein markers
Immunocytochemistry	0h, 2h, 16h, 24h	Cellular viability and expression/localization of relevant ER stress/UPR protein markers
qPCR	24h	Expression of relevant UPR/Proteostasis/Aging gene markers
Trypan Blue® cell counting	No timepoints	Initial cell seeding for posterior assays
BCA Protein Assay	No timepoints	Total protein content quantification

4 Results

4.1 Drug dose curve

To better assess optimal dosage for cell treatments in following procedures used in this report, a dose curve for all compounds used was established. Prior to empirical experiments, literature revision was done to better comprehend in which range of concentrations these compounds should be used without major cytotoxic damage. This literature revision was performed mainly using PubMed (National Center for Biotechnology Information, U.S. National Library of Medicine), discussed and reviewed before any *wet lab* testing.

Following data collection and analysis, to every compound, aspects such as initial cell numbers, biological replicas and timepoints were standardized across all used compounds. Every compound concentration and respective control were assessed using the resazurin method and cell were seeded at $8.5x10^4$ cells.cm^{-2} as detailed in section 3.2.

4.1.1 Thapsigargin dose curve

As already mentioned in section 3.2, TG is one of the most efficient drugs to induce ER stress in cells, hence the dose curve to optimize working concentrations. To minimize cell population variables, cells were incubated in quadruplicate. Negative control cells were maintained with culture medium without supplement restrictions, which was replaced by fresh medium at the time of compound application. Different TG concentrations were as follows: 10 nM, 50 nM, 100 nM and 1000 nM. To achieve correct concentrations, serial dilutions was performed. A 5 mM stock solution was used to achieve the highest working concentration, which in this case was of 1000 nM, while lower working concentrations were achieved through dilution of 1000 nM working solution. Figure 16 illustrates metabolism values, in percentage, compared to control levels.

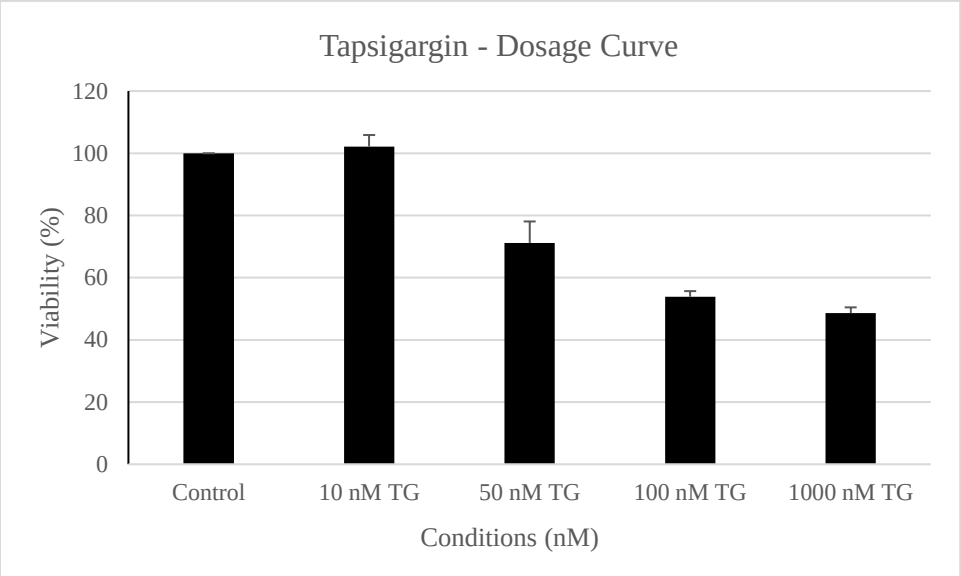

*Figure 16 - **Thapsigargin dosage curvet in SH-SY5Y cells**. Viability was assessed using resazurin assay) after cell incubation with different thapsigargin concentrations (0 nM;10 nM ;50 nM; 100 nM;1000 nM) for 24h. Data is presented in percentage mean values with their respective standard deviation. Mean values were obtained from n=4 replicas.*

As expected, increasing concentrations of thapsigargin induce higher cytotoxic damage which in turn induce cell death, resulting in a lower viability percentage (Figure 16). Also, common working concentrations for thapsigargin are close to 100 nM, concentration present in this assay. With a 53% cell viability, a significant cell stress and cytotoxicity is achieved without overkill of that same cell population and confirm that 100 nM TG is an effective concentration to study ER stress.

To better understand at what timepoints does 100 nM TG concentration has a more severe effect on SH-SY5Y and to better understand optimal timepoints for cell incubation for this ER stress inducer, a similar assay was performed using two different timepoints: 16 hours and 24 hours. Using only 100 nM TG concentration, viability values were obtained from a quadruplicated replica (Figure 17).

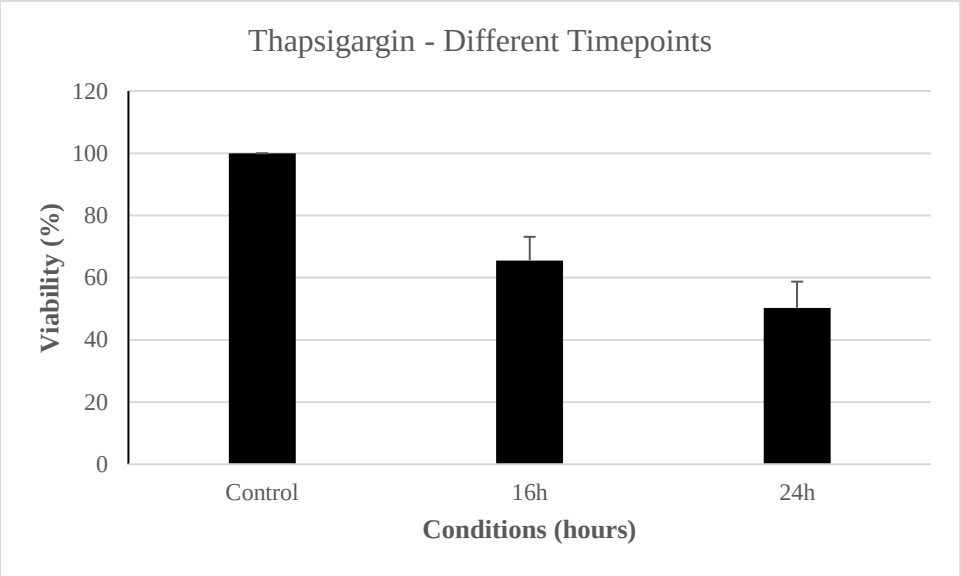

Figure 17 - Viability values at different timepoints for 100 nM TG concentration, in SH-SY5Y cells. N=4. Data is presented in percentage mean values with their respective standard deviation.

As expected, increased exposure time results in lower viability values and, consequently, in higher cell death. However, since exposure times for thapsigargin are normally of 24 hours or more are used (based on literature review) and since a 50% viability was achieved after 24 hours, this timepoint was considered optimal for further incubations with this reagent, without causing excess cell death.

4.1.2 Tunicamycin dose curve

TUN is the other ER stress inducer for SH-SY5Y cells. To determine optimal concentration levels, this initial protocol similar to the TG procedure done in 4.2.1, considered various TUN concentration values and respective cell metabolism through resazurin method, assessed in quadruplicate. As for concentration intervals, the following values were used: 0.1 µg. mL^{-1}, 1 µg. mL^{-1}, 3 µg. mL^{-1} and 5 µg. mL^{-1}. Serial dilutions were performed from a 10 mg. mL^{-1} stock solution to achieve the highest working concentration. 5 µg. mL^{-1} solution was used to achieve the other concentrations. Negative control cells were maintained with culture medium without supplement restrictions, which was replaced by fresh medium at the time of compound application. Figure 18 illustrates metabolism values, in percentage, compared to control conditions.

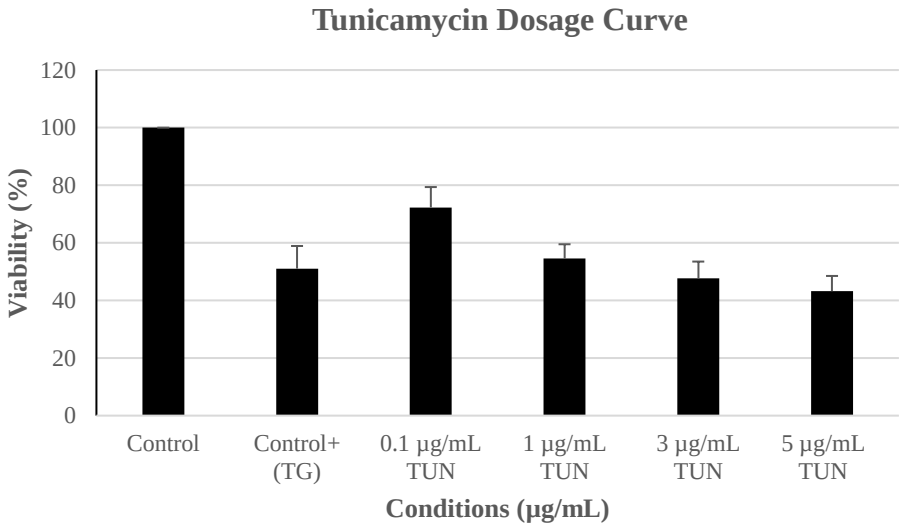

*Figure 18 - **Tunicamycin dosage curve.** SH-SY5Y cells were exposed to different TUN concentrations (0.1 µg. mL^{-1}, 1 µg. mL^{-1}, 3 µg. mL^{-1} and 5 µg. mL^{-1}) and to 100 nm TG as a positive control, for 24 hours. N=4. Data is presented as mean values from replicas and respective standard deviations.*

Crescent concentrations seem to have a crescent effect in cell death and consequently, a diminishing effect on cell viability. Literature review stated 1 µg. mL^{-1} TUN as a common working concentration. Figure 18 evidently shows a successful induction of cell stress based on its 54% cell viability, showing also that no excess cell death occurs, and minimal cell quantity is maintained, having similar values to its 100 nM TG counterpart, proving its suitability for further experimentation.

4.1.3 TUDCA reversion of ER stress-induced cytotoxicity

In the same way ER stress inducers were scrutinized to better understand cytotoxic effects in SH-SY5Y, TUDCA was evaluated to better understand its influence in viability amelioration and overall cell stress reversion. Since it is proven TUDCA has beneficial effects in ER stress context, different TUDCA concentrations that were non cytotoxic, were used to better analyse its effects. Cells were assessed in quadruplicate by resazurin assay and the following TUDCA concentrations were used: 100 µM, 250 µM, 500 µM, 1000 µM. A negative control composed of the same cell number but with fresh normal medium was used. A 100 nM thapsigargin concentration was used to Figure 19 illustrates plate scheme and respective viability graphic.

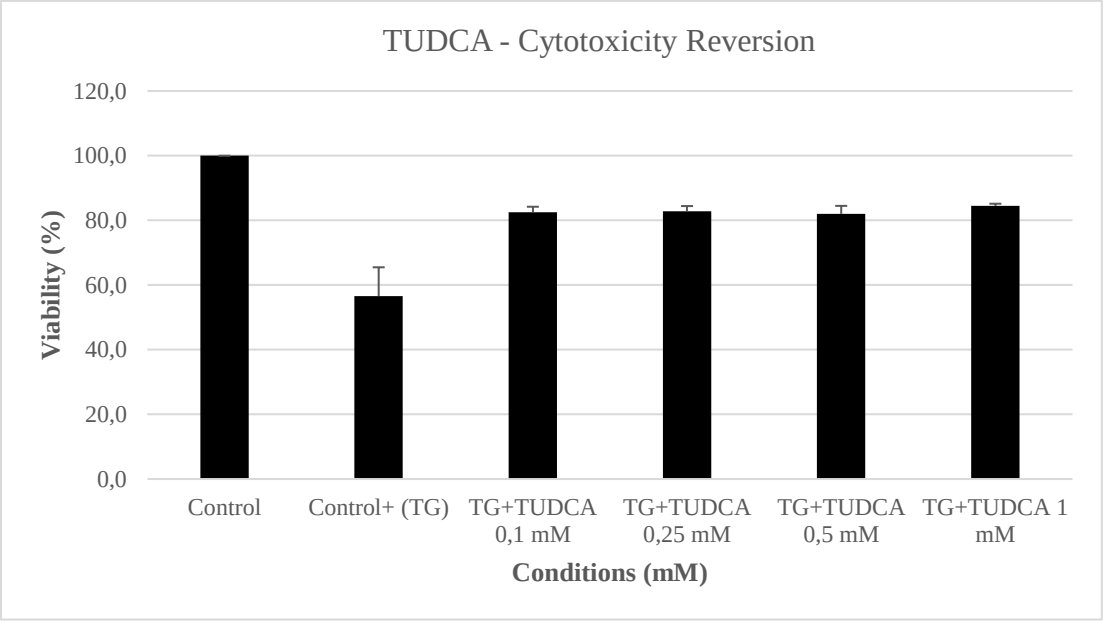

*Figure 19 - **TUDCA cytoxicity reversion in the presence of an ER stress inducer (TG).** Crescent TUDCA concentrations were analysed (100 µM, 250 µM, 500 µM, 1000 µM.) to a quadruplicated replica (N=4). 100 nM TG was used as ER stress inducer.*

In the presence of an ER stress inducer such as TG, TUDCA seems to have a role in diminishing cell stress ratios and therefore ameliorating cell viability percentages. Indeed, TUDCA presence results in a viability value of approximately 20% more, when compared to condition where only TG is present. However, crescent concentrations of this compound have little to no effect on the viability values and, therefore, an ideal TUDCA concentration of 0,1 mM was considered the most adequate for future experimentation.

4.2 Fluorescence cytochemistry

In the work reported by Verwilst et al, 2019, a thioflavin fluorescent chemosensor was developed to detect protein aggregates in HeLa cells and reported a dramatic increase of fluorescence when ER stress was induced with TG[101]. Here, a cytochemistry-based assay was performed to confirm the presence or absence of protein aggregates in SH-SY5Y cells after incubation with both ER stress inducers (TUN and TG). To this end, the golden standard Proteostast dye was used to effectively assess the presence of protein aggregates. Two different concentrations for both thapsigargin (100 and 1000 nM) and tunicamycin (at 1 and 5 µg/mL) were used, and cells exposed for 24h. In all conditions assessed, no significant protein aggregation was detected in either compound or concentration, as

depicted in Figure 20. Compared to positive control (MG132), both thapsigargin and tunicamycin do not appear to significantly induce protein aggregation in the conditions tested.

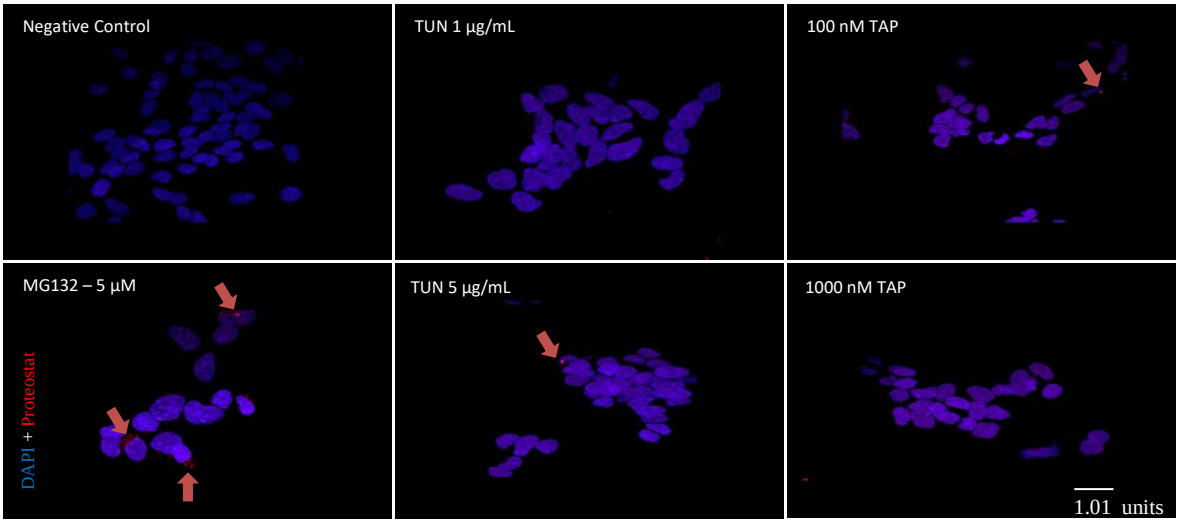

Figure 20 - **Confocal microscopy microphotographs of cellular protein aggregates in SH-SH5Y cells exposed to TG and TUN.** *Cells were incubated for nuclei after a 24h incubation with the ER stress inducers TG (100 and 1000 nM) and TUN (at 1 and 5 µg/mL). Nuclei is marked with DAPI (in blue) and protein aggregates are marked with Proteostast (in red). Arrows indicate areas of protein aggregates.*

4.3 Total protein quantification assay

As mentioned in section 3.2.3., a protein quantification assay based on bovine serum albumin was performed to accurately precise protein concentration that are necessary for subsequent SDS-PAGE. Figure 21 illustrates mean values of four biological determinations, using two technical replicas in each. This ensures that further loading in SDS-PAGE gels is mass normalized and with the least variability possible. Total protein content tends to diminish as seen in Figure 21 across conditions incubated with the ER stress inducer TUN, even in the presence of the protective compounds.

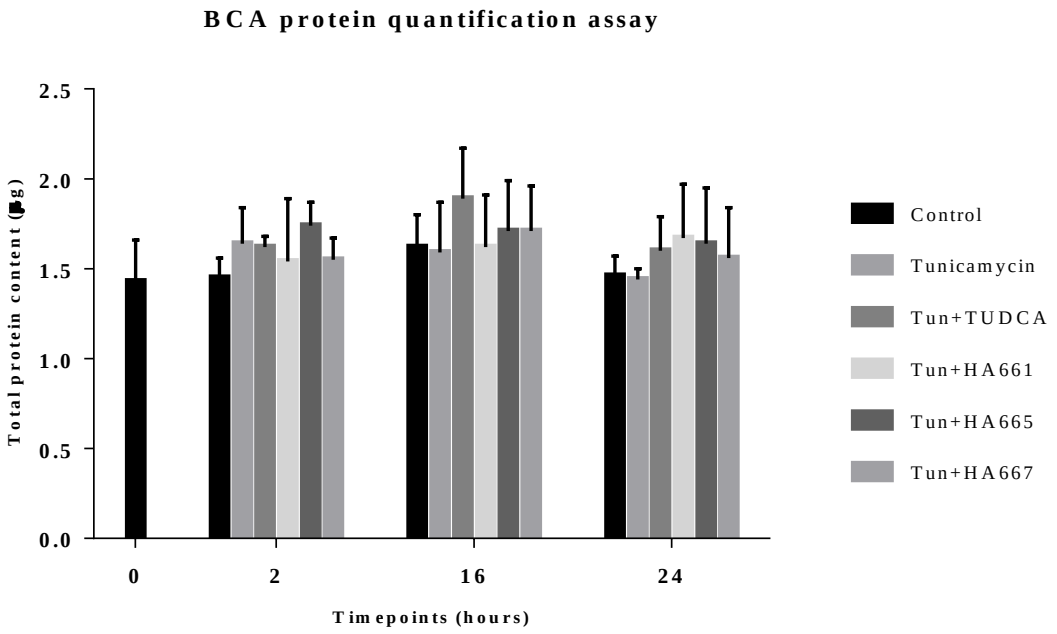

*Figure 21- **Total BCA Protein concentration quantification assay values of cells' lysates after incubation with TUN alone or in combination with the protective compounds (TUDCA and HA compounds).** Values are shown as the mean of all replicas (n=4) and respective SD.*

4.4 RT-qPCR Target Genes activity

To confirm that the proposed cell model of ER stress induction and reversion is effective, a gene expression analysis done to evaluate genes of interest related to UPR at the transcript level. To achieve this, six conditions, three control samples (CTRL cells and cells exposed only to Tun or TG) and three treatment samples (TUN+TUDCA; TUN+665; TG+665), were seeded and incubated (details in section 3.2.7). Cells were thereafter lysed and homogenized, and their total RNA isolated to further quantification using NanoDrop (Table 5).

Table 7 - ***Summarization of NanoDrop values and respective total RNA concentration for further calculation.*** *$OD_{260/230}$ ratios indicate possible phenol contamination and should not exceed a value of 1.6. $OD_{260/280}$ indicate possible DNA contamination and should not exceed 1.9.*

Conditions	OD (260/230)	OD (260/280)	Total RNA concentration (ng/µL)
Control	2.214	2.131	1335.411
1 µg/mL TUN	2,115	2.115	1368.826
100 nM TG	2.218	2.181	843.960
1 µg/mL TUN + 0,1 mM TUDCA	2.098	2.175	1423.286
100 nM TG + 50 µM HA665	1.999	2.137	461.439
1 µg/mL TUN + 50 µm HA665	1.295	2.011	112.956

Normalization of total RNA amount (0.75 µg total RNA) between all conditions, was done before mRNA reverse transcription to cDNA, in order to achieve a proper comparison between samples after reverse transcription. Following reverse transcription, qPCR was performed. Figure 24 depicts calreticulin and GRP 78 normalized relative expression levels based on values obtained when compared to gene expression levels of Hrtp1, the housekeeping gene used as positive control. In the same way, Figure 25 illustrates the normalized relative expression profile of CHOP and the XBP1s.

Regarding calreticulin and XPB1s, it seems that inducing ER stress through either TG or TUN increase gene expression and respective mRNA levels which are promptly followed by a decrease of those values in conditions where protective agents (TUDCA and HA665) were present. Figure 22a also shows that the TUDCA seems to be more effective at diminishing calreticulin expression levels when compared to HA665. On the other hand, HA665 seems to have a more potent effect on diminishing XBP1s values when TUN is used as a stress inducer rather than TUDCA (Figure 23). However, in the presence of TG, HA665 seems to have no effect on XBP1s expression.

Regarding GRP78, depicted in figure 22b, conditions induced only with TG or TUN increase relative expression values, when compared to negative control. It seems that the presence or absence of protective agents, either TUDCA or HA665, has no diminishing effect on GRP78 expression levels. More, it seems that the presence of protective agents

increases GRP78 expression values slightly, indicating that these are active and upregulated despite ER stress ameliorators.

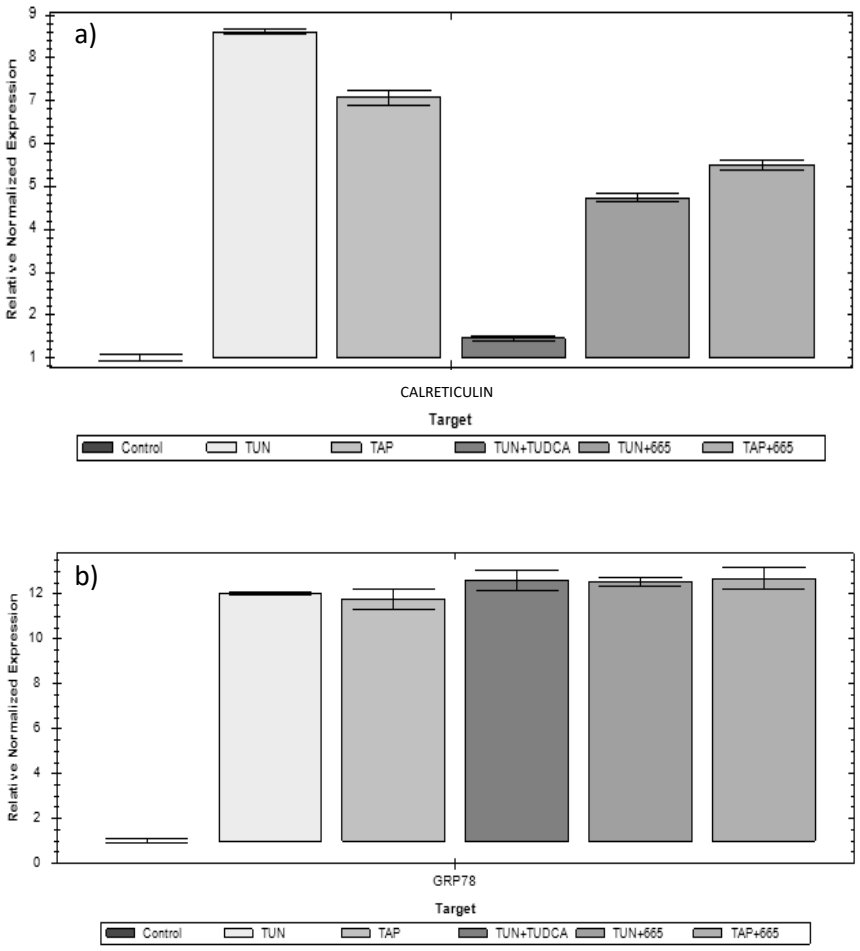

Figure 22 - ***Relative normalized expression values obtained for a) calreticulin and b) GRP78.*** *N=1 with two technical replicas. Values are shown as relative values compared to control housekeeping gene Hrtp1 and normalized against negative control.*

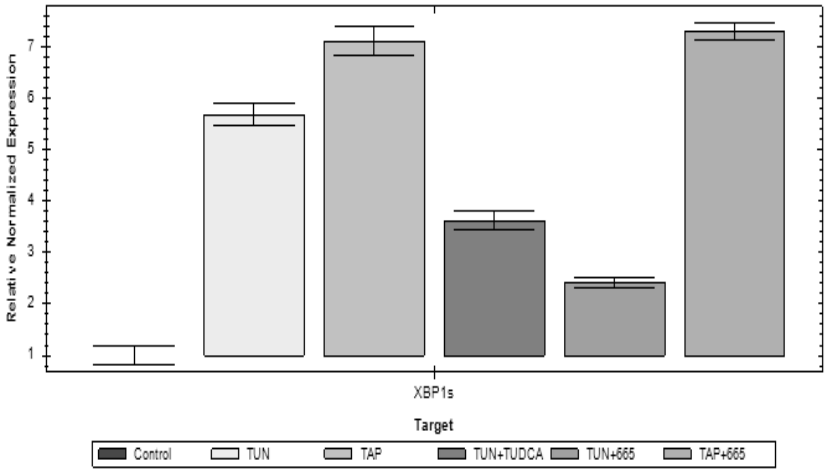

*Figure 23 - **Relative normalized expression values obtained for XBP1s.** N=1. Values are shown as relative expression values compared to control housekeeping gene Hrtp1 and normalized against negative control.*

4.5 Immunoblot

The induction of ER stress and associated aging pathways as well as UPR pathways in SH-SY5Y cells incubated with TUN and TG, was confirmed by evaluating expression levels (at protein level) of key proteins by immunoblot. To better characterize the state of UPR activity and of aging associated pathways, protein profiles of aging associated proteins such as pERK/ERK, UPR proteins such as ATF4, and the proteostasis-associated protein BAG3, were analysed.

First, the ER stress inducer used, thapsigargin, was used at a 100 nM working concentration. Incubation time was for 2 hours, known to be the peak of ATF4 expression. Results (Figure 24) evidence an early activation of both ATF4 and pERK/ERK, indicating a clear early response to the induced stress environment. ATF4 expression levels rise especially high in TUN condition with no protective agents, while the presence of those same protective agents significantly diminish ATF4 values. The ratio between the activated form of ERK, known as pERK and total ERK content indicates the activation or inhibition of this protein. Figure 24 evidently shows that ER stress conditions such as the ones induced by TG also induce the activation of ERK and consequently, of its phosphorylated form, hence its high ratio value. Presence of protective agents seem to have a role in the inhibition of ERK phosphorylation even in the presence of TG.

On the contrary, BAG3 seems to have little upregulation of its expression levels at early stages of cellular stress, increased in conditions where compounds that alleviate stress by protein aggregation are present.

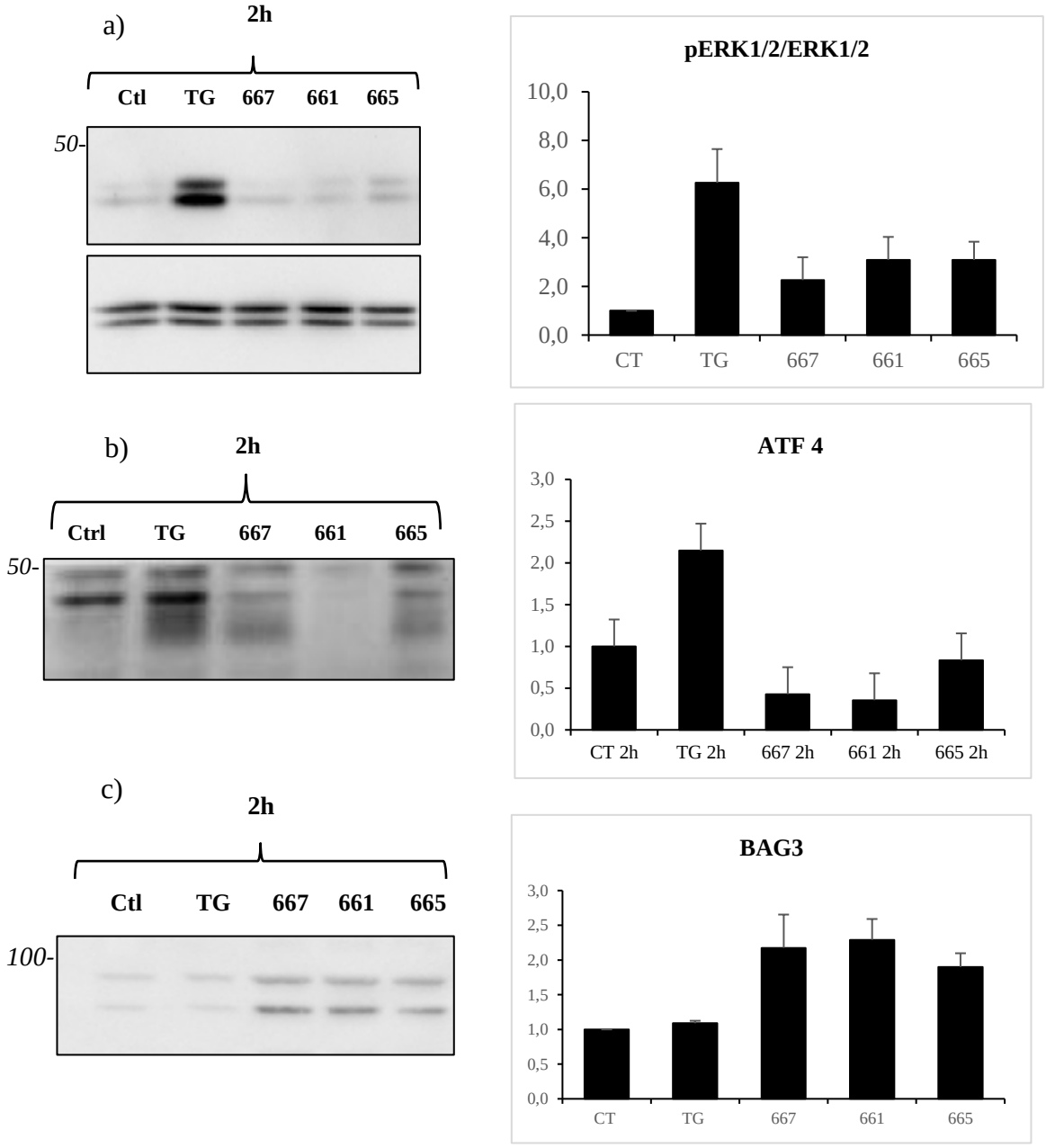

Figure 24 - ***Representative band images and respective fold increase values for a) ATF4, b) pERK/ERK and c) BAG3 after a 2h incubation with TG (100 nM) and HA Compounds (50 µM).*** *Quadruplicated replica. Data is shown as fold increase when compared to control condition.*

An expanded temporal profile was constructed based on a different ER stress inducer, tunicamycin. Target proteins were BAG3 and ATF4 (Figure 25). Cells were incubated with the indicated compounds for 2, 16 and 24 hours, before sample collection. Classical SDS-PAGE and immunoblot were performed, and band densities further quantified. Similar to the first band images from thapsigargin, ATF4 has an earlier fold increase peak

profile, maxing at 2 hours. Also concurrent to thapsigargin results, BAG3 seems to have little increase at earlier stages of ER stress environment. However, its temporal profile increases slightly at 16 hours and 24 hours. Protective agents seem to have little to no effect on BAG3 fold increase values.

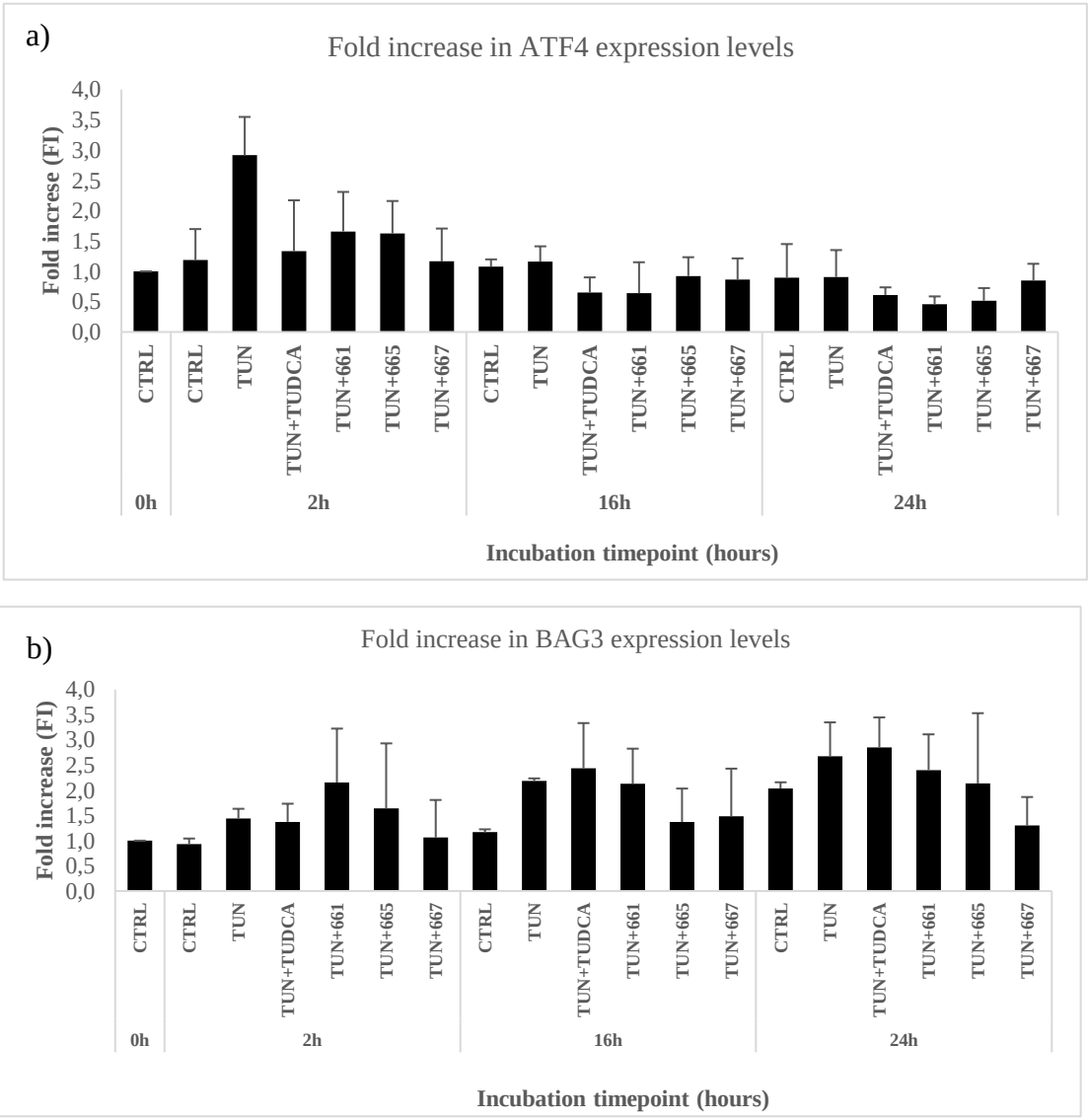

Figure 25 - ***Temporal profile for (a) ATF4 and (b) BAG3 expression levels after a 2 hour, 16 hour and 24 hour incubation with TUN (1 µg/mL), HA compounds (50 µM) and TUDCA (0,1 mM).*** *N=4. Data is shown as fold increase when compared to control condition (that is, immediately collected after incubation)*

5 Discussion

In this work, aiming to study the effect of ER stress and its impact on pathways related to aging and proteostasis, we first performed several metabolic viability assays for different ER stress inducers (TG and TUN) and modulators (TUDCA) to confirm effective induction of ER specific stress and consequent cell death (or protection against it). Results obtained show that a 24 hour incubation with either ER stress inducer (TG and TUN) is sufficient to effectively induce cytotoxicity and cell death, while at the same time crescent thapsigargin or tunicamycin concentrations result in increased cell death (and as so, in less cell viability), with minimum values of 48% and 43% viability, respectively, for the highest concentrations used (1000 nM TG and 5 µg. mL^{-1} TUN). Data obtained also showed that concentrations of 100 nM TG and 1 µg. mL^{-1} TUN are sufficient to reduce cell viability percentage by half, confirmed by their 53% and 54% values.

Comparing to literature, different approaches, concentrations and timepoints are used for TG. While some reports use lower timepoints with longer checkpoints to achieve significant ER stress levels, concentration for thapsigargin varies from 0.1 µM to 10 µM with varying timepoints ranging from 4 hours to 48 hours with a mild success in ER stress induction[102,103], being concurrent with working concentrations used here for TG. Regarding cell viability specifically, a report using 100 nM TG and incubation time of 70 hours in a MCF7 line achieved a final viability percentage of ~50%[103]. Other report described an incubation of SH-SY5Y cells with 100 nM TG for 16 hours with viability results around 75%[104]. Timepoints used greatly influence cell viability even for a similar concentration and, therefore, values obtained in this report are considered a good indicator of ER stress induction by thapsigargin. Regarding

tunicamycin and cell viability, a report using a 48-hour timepoint with a 2 mg/mL TUN concentration achieved cell viability values of ~20%. 20% viability in 48h is somewhat in accordance and proportional to the results obtained. Other reports with values and concentrations similar to the ones here used obtained similar results to the ones we have obtained(?). For instance, a report using a 24-hour timepoint with varying concentrations achieved a cell survival percentage, through SRB (Sulforhodamine B) assay, of ~50% and ~30% for conditions treated with, respectively, 1 µg.mL^{-1} and 4 µg.mL^{-1} TUN[105]. These findings are concurrent with data obtained in this report and further confirm 1 µg. mL^{-1} as a good concentration value for ER stress induction through tunicamycin without excess cell death.

An increase in metabolic viability using the neuroprotective agent TUDCA in the presence of TG as the ER stress inducer, supported that TUDCA may have a cell protective role as a general chaperone (Figure 19). TUDCA is included in the category of hydrophobic chemical chaperones, which, by classical definition, regulate the process of protein folding and assembly, thus preventing their degradation or aggregation and guaranteeing their correct functionality[106]. The mode of action of TUDCA and its consequent cytoprotective effect relies mainly on the reduction of ROS formation[107] and in the inhibition of apoptosis in both extrinsic[108] and intrinsic[109] pathways. TUDCA is also capable of activating nuclear receptors and G protein-coupled receptors, therefore regulating gene expression, more specifically of genes encoding proteins involved in the regulation of glucose, fatty acids and lipoprotein synthesis[110]. *In vitro* data described in a particular report[111] support these prior statements. In spite of using pre-incubation times of 1h and concentrations at the millimolar interval, far superior to the ones used here, TUDCA successfully prevented aggregation of different proteins, through regulation and suppression of the mRNA levels of GRP78 and other ER chaperones[111]. Interestingly in this report, TUDCA had a much more potent effect in preventing incorrect folding in the presence of TUN rather than in the presence of TG, while here, only calreticulin was effectively reverted by TUDCA. This may be related to the fact that these ER stress-inducers have specific modes of action that influence TUDCA's chaperone activity. Since TUN relies on the inhibition of glycosylation of newly synthetized ER proteins, TUDCA, having an

amphiphilic structure, binds to the hydrophobic parts of the aggregated protein and prevents incorrect folding, therefore suppressing TUN-induced GRP78 expression. On the other hand, TG depletes ER calcium levels, which are important for the binding of GRP78, GRP94 and calreticulin, which are calcium-dependent chaperones[112]. A depletion in calcium levels would activate UPR regardless of TUDCA presence, which strangely, in this report, was not observed for TUN induced cells, since TUDCA was unable to revert GRP78 expression levels, with a need for additional research to confirm TUDCA interaction with GRP78, perhaps with higher scale working concentrations.

Fluorescence cytochemistry was performed using Proteostat dye to evaluate protein aggregation under ER stress caused by either TG or TUN. Crescent concentrations of both ER stress inducers proved to be insufficient to cause significant protein aggregation (Figure 20). As stated in section 4.2., this assay was performed based on reports that described successful detection of protein aggregation after thapsigargin and tunicamycin incubation (Section 4.2.). Indeed, several reports indicate significant protein aggregation when incubated with either thapsigargin or tunicamycin. Even for small concentrations, protein aggregation was detected through microscopy or other assays in cells exposed to TUN[113] and TG[101]. Results obtained here show that other mechanisms are being activated by ER stress inducers. As stated before, TG and TUN each uniquely inhibit sarco-endoplasmic reticulum Ca^{2+} channels and, therefore, block the ER ability to sequester and remove cytosolic Ca^{2+} to the extracellular environment in order to maintain calcium homeostasis, resulting in an increase of free cytosolic calcium levels[114,115]. Free cytosolic calcium levels have several consequences: increased ROS activity, inhibition of catalase activity and activation of Ca^{2+}-dependent apoptosis[116]. The absence of protein aggregates and peculiar nuclear morphology (Figure 20) depicted from DAPI staining here reported can elucidate that, despite promoting protein aggregates, TG and TUN possibly induce Ca^{2+}-dependent apoptosis by blocking ER calcium storage and consequently raise cytosolic free calcium. One method to better assess this possibility would be the evaluation of ROS activity through proper quantification assays and with higher concentrations of TUN and TG.

Total protein quantification assay was performed prior to SDS-PAGE and WB procedure in order to normalize protein content to all conditions. Also, this quantification helps to elucidate if protein synthesis is up or downregulated between conditions or between timepoints, based on total protein content. Literature states an increase of protein synthesis following ER stress induction, specifically through ATF4 and CHOP, which regulate ER stress-mediated cell death and share target genes for protein synthesis[117]. Protein synthesis is also related to cell death, consequence of ATF4 and CHOP activity which increase ROS activity and consequent apoptosis[118]. As figure 21 shows, protein content in this case was not significantly higher between control and conditions of ER stress induction, at any of the different timepoints of cells exposure (Figure 21), compared to control, indicating that protein synthesis is approximately constant.

To further assess if our TUN/TG-exposed SH-SY5Y cells are good cell models for studying ER stress induction and reversion, the levels of calreticulin, GRP78 and XBP1s mRNAs were obtained by RT-qPCR, as shown in figure 22 and 23. In the presence of ER stress inducers TUN and TG, these proteins were expected to raise their expression levels in response to the stressful environment. Calreticulin acts as a Ca^{2+}-binding chaperone and acts a regulator of protein quality and folding control alongside calnexin, while also having a role in ER stress attenuation by autophagy induction, and is highly activated by either TG or TUN, as previously reported[119]. Indeed, figure 22a shows a clear increase of calreticulin expression levels in TG or TUN treated conditions. Calreticulin expression levels are reduced in conditions treated with neuroprotective agents, specifically in TUDCA treated cells (Figure 22a), which indicate a somewhat successful reversion of ER stress by the compounds. In-house developed HA665 was also able to reduce stress-induced calreticulin, but TUDCA was a stronger ameliorator, reverting calreticulin levels to almost basal ones. Similar patterns were observed for TUN-induced XBP1s expression levels, but HA665 was unsuccessful in reverting XBP1s expression levels in TG treated conditions. As stated before, the UPR branch of IRE1 is activated during ER stress and processes XBP1s mRNA to form its spliced form, XBP1s. The ratio between the normal and spliced XBP1 form correlate to the amount of expressed proteins that are present to

adapt the ER to the stressful environment[120]. TG treated conditions seem to have no effect in XBP1s expression levels when HA665 is present. However, additional evaluations specifically with this in-house developed compound are needed.

ER stress induction causes an increase in GRP78 gene expression levels as expected (figure 22), meaning that GRP78 expression is induced in response to the stressful environment. However, it seems that TUDCA or the HA655 compound have no influence in ameliorating this protein's expression levels. This might be due to the fact that GRP78 presents, as stated in 1.2.4., in two major states: oligomeric and monomeric. While in the absence of neuroprotective agents, GRP78 is highly dissociated from UPR branch receptors and has a stronger affinity with unfolded proteins, explaining its rise even after UPR translational modifications in this gene. In the presence of these neuroprotective agents, ER stress is diminished although GRP78 continues to be highly expressed post-response to a more oligomeric dominant state, which has a much higher affinity with the UPR branch receptors and, consequently, diminishing unfolded protein and ER response.

Immunoblot assays were performed, as mentioned above, to evaluate protein levels of proteostasis and aging-related targets such as BAG3, ATF4, ERK1/2 in ER stress environments. ATF4 was chosen to better assess if ER stress was present on treated conditions. ATF4 seems to have an earlier peak, increasing significantly at 2h and decaying at the following timepoints (Figure 25a). TUN induced ER stress increases ATF4 levels, since it activates one of UPR branches, specifically the PERK-CHOP-ATF4 pathway. The neuroprotective agents tested decreased ATF4 levels, which indicates a (at least partial) reversion of ER stress. ATF4 is a rather early acting protein in the PERK-ATF4-CHOP pathway cascade (Figure 26), targeting other proteins to induce vesicle elongation and increase autophagy levels by aiding in the genesis and maturation of the autophagosome[122], possibly explaining its increased values at earlier incubations stages.

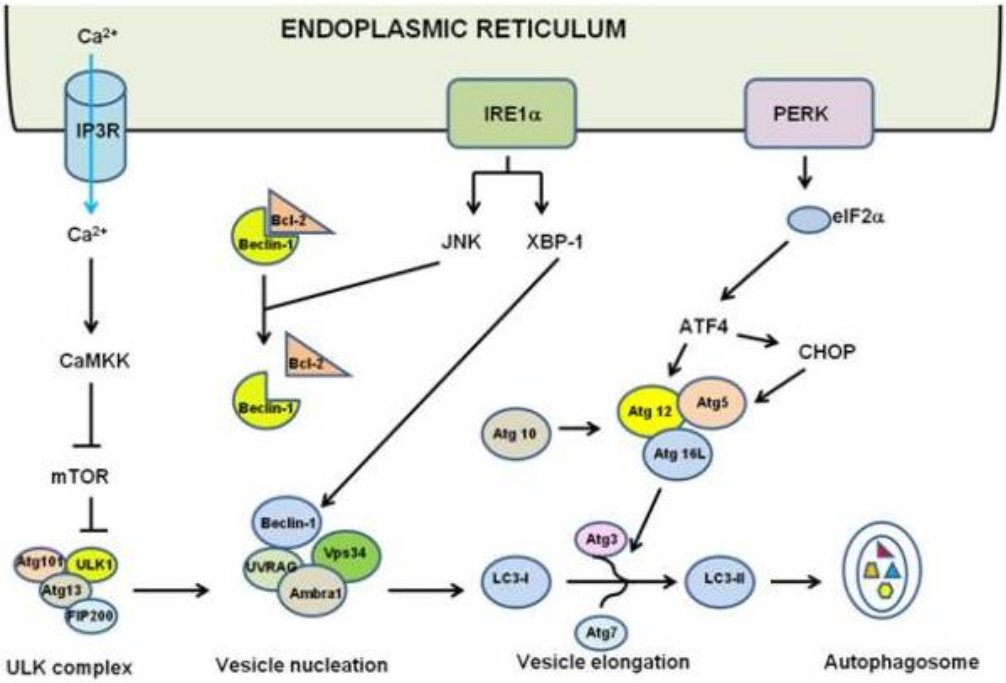

Figure 26 - UPR branches in autophagy context124

BAG3 temporal profile shows that only in the presence of TUN at 2 hours, this protein is increased. The presence of neuroprotective agents does not have a decrease, rather an increase, in BAG3 values at 2h. At 16h and 24h, TUDCA seems to have no effect in BAG3 levels and HA compounds seems to slightly increase its relative expression levels, except for one or two conditions (Figure 24 and 25). BAG3, as already stated before, is a co-chaperone that is involved in protein folding, while also being implicated in activating non-conventional autophagy pathways, specifically when linked with HSP70, and its ratio comparatively to BAG1 greatly increases in pathophysiological conditions such as ER stress[123]. Its temporal profile (Figure 25b) shows that at later incubation timepoints such as 16h and 24h positive control conditions, BAG3 levels slightly increase, but more in TUN-induced stress conditions. This might be due to the fact that BAG3 presents itself as a co-chaperone who can associate, similar to its association with HSP70, with TUDCA and HA compounds, explaining its slight increase in the presence of these agents. However, additional studies concerning selective autophagy and chaperone-mediated protein folding

quantifications are needed to see if BAG3 is influenced by the neuroprotective compounds.

Finally, the ERK pathway was also analysed by Western Blot analysis. As stated in section 1.3., ERK1/2 has direct links with cell lifespan and longevity through its action in cellular senescence, proliferation and differentiation. The activation of this pathway shows (Figure 24) a clear increase in conditions treated with TG and is promptly reduced by in-house developed compounds at early stages of its phosphorylated state (activation). This might indicate that ERK1/2 are activated upon ER stress and participate in a possible pathway to ameliorate this environment. Evidence state a non-canonical CHOP pathway in which ERK1/2 participates. AngioGenic Factor 1 (AGGF1) seems to induce expression of miR-183-5p which in turn reduces CHOP expression (Figure 27). At the same time, the presence of this angiogenic factor inhibits ERK1/2, leading to a decrease of the transcriptional repressor Zinc Finger E-Box Binding Homeobox 1 (ZEB1), increasing miR-183-5p and leading to an even higher decrease of CHOP levels[124]. This might explain that, similar to AGGF1, HA compounds repress ERK1/2 activation. However, more studies are needed to evaluate how HA compounds and TUDCA might regulate ERK1/2 levels.

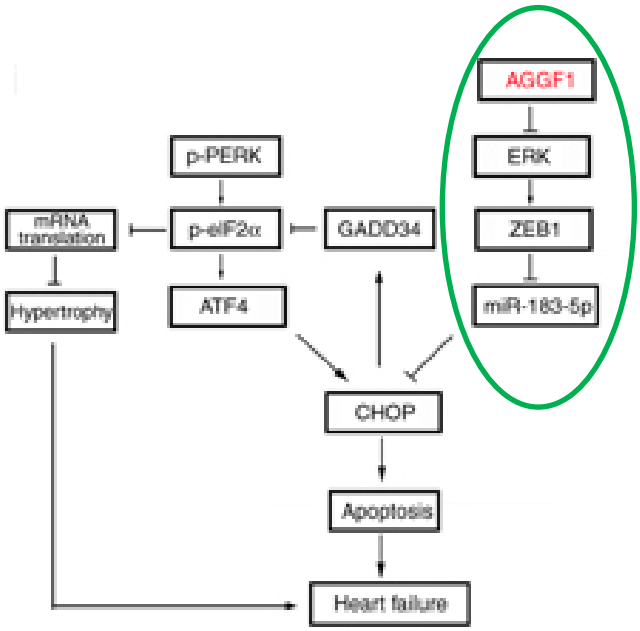

Figure 27- Non-canonical CHOP-ERK1/2 pathway[124]

6 Conclusion

Here, we propose a cell model using SH-SY5Y neuronal line to adequately illustrate ER stress environments and its chemical reversion using neuroprotective compounds such TUDCA and homegrown protein aggregate reversers known as HA compounds while also stating this ER stress impact on pathways related to aging and protein homeostasis. Although not at a universal scale, we show that SH-SY5Y cells are adequate to show variable ER stress related proteins and respective gene expression levels across different conditions used. Several techniques were used to ensure the analysis of multiple biological outcomes. Calreticulin, ATF4 and BAG3 seem to be good indicators of ER stress. However, additional studies and replicas for XBP1s, CHOP, GRP78 and pERK are needed to confirm that all branches of UPR and at the same time, the proteostasis network, are indeed all affected, since no significant results were achieved to these specific targets, except for pERK, who only lacks an adequate temporal profile similar to BAG3 and ATF4 (figure 25).

As for future work and side note, qRT-PCR might not be an optimal assay to evaluate gene expression levels using SH-SY5Y, since several attempts were performed to achieve significant results with little to no success, especially in RNA isolation phase. Other techniques such as column chromatography would probably achieve better results since the target proteins would be in a much pure state to further quantify. Also, fluorescence microscopy studies largely state the presence of protein aggregation foci due to ER stress induction using either TG or TUN, as stated in section 5. This requires additional microscopy protocols to be performed using SH-SY5Y, using a fluorescent chemosensor such as the ones used by Verwilst et al, 2019, which served as the main product to evaluate protein aggregates in this report. Finally, other target proteins such as mTOR, HSP70 and

other BAG proteins should be thoroughly studied by similar assays used here and using this cell line to confirm its status as a good cell model for the evaluation of ER stress.

7 References

1. Cornelissen, G. & Otsuka, K. Chronobiology of Aging: A Mini-Review. *Gerontology* **63**, 118–128 (2017).
2. Pan, H. & Finkel, T. Key proteins and pathways that regulate lifespan. *J. Biol. Chem.* **292**, 6452–6460 (2017).
3. López-Otín, C., Blasco, M. A., Partridge, L., Serrano, M. & Kroemer, G. The hallmarks of aging. *Cell* **153**, 1194–217 (2013).
4. Ferrucci, L., Giallauria, F. & Guralnik, J. M. Epidemiology of aging. *Radiol. Clin. North Am.* **46**, 643–52, v (2008).
5. Ine, I. N. D. E. Dia Mundial da População 11 julho de 2014 População residente em Portugal com tendência para diminuição e envelhecimento. *Destaque* 1 (2014).
6. Aunan, J. R., Watson, M. M., Hagland, H. R. & Søreide, K. Molecular and biological hallmarks of ageing. *Br. J. Surg.* **103**, e29–e46 (2016).
7. Hanahan, D. & Weinberg, R. A. Hallmarks of Cancer: The Next Generation. *Cell* **144**, 646–674 (2011).
8. Powers, E. T., Morimoto, R. I., Dillin, A., Kelly, J. W. & Balch, W. E. Biological and Chemical Approaches to Diseases of Proteostasis Deficiency. *Annu. Rev. Biochem.* **78**, 959–991 (2009).
9. Klaips, C. L., Jayaraj, G. G. & Hartl, F. U. Pathways of cellular proteostasis in aging and disease. *J. Cell Biol.* **217**, 51–63 (2018).
10. Labbadia, J. & Morimoto, R. I. Proteostasis and longevity: when does aging really begin? *F1000Prime Rep.* **6**, 7 (2014).
11. Díaz-Villanueva, J. F., Díaz-Molina, R. & García-González, V. Protein Folding and Mechanisms of Proteostasis. *Int. J. Mol. Sci.* **16**, 17193–230 (2015).
12. Martínez, G., Duran-Aniotz, C., Cabral-Miranda, F., Vivar, J. P. & Hetz, C. Endoplasmic reticulum proteostasis impairment in aging. *Aging Cell* **16**, 615–623 (2017).
13. Kwon, Y. T. & Ciechanover, A. The Ubiquitin Code in the Ubiquitin-Proteasome System and Autophagy. *Trends Biochem. Sci.* **42**, 873–886 (2017).

14. Bragoszewski, P., Turek, M. & Chacinska, A. Control of mitochondrial biogenesis and function by the ubiquitin-proteasome system. *Open Biol.* **7**, (2017).

15. Sands, W. A., Page, M. M. & Selman, C. Proteostasis and ageing: insights from long-lived mutant mice. *J. Physiol.* **595**, 6383–6390 (2017).

16. Kleiger, G. & Mayor, T. Perilous journey: a tour of the ubiquitin-proteasome system. *Trends Cell Biol.* **24**, 352–9 (2014).

17. Tonoki, A. *et al.* Genetic Evidence Linking Age-Dependent Attenuation of the 26S Proteasome with the Aging Process. *Mol. Cell. Biol.* **29**, 1095–1106 (2009).

18. Kruegel, U. *et al.* Elevated Proteasome Capacity Extends Replicative Lifespan in Saccharomyces cerevisiae. *PLoS Genet.* **7**, e1002253 (2011).

19. Liu, H.-Y. & Pfleger, C. M. Mutation in E1, the Ubiquitin Activating Enzyme, Reduces Drosophila Lifespan and Results in Motor Impairment. *PLoS One* **8**, e32835 (2013).

20. Min, J.-N. *et al.* CHIP deficiency decreases longevity, with accelerated aging phenotypes accompanied by altered protein quality control. *Mol. Cell. Biol.* **28**, 4018–25 (2008).

21. Mizushima, N. & Komatsu, M. Autophagy: Renovation of Cells and Tissues. *Cell* **147**, 728–741 (2011).

22. Fîlfan, M. *et al.* R RE EV VI IE EW W Autophagy in aging and disease. *Rom J Morphol Embryol* **2017**, 27–31

23. Loos, B., Engelbrecht, A.-M., Lockshin, R. A., Klionsky, D. J. & Zakeri, Z. The variability of autophagy and cell death susceptibility: Unanswered questions. *Autophagy* **9**, 1270–85 (2013).

24. Li, W., Li, J. & Bao, J. Microautophagy: lesser-known self-eating. *Cell. Mol. Life Sci.* **69**, 1125–1136 (2012).

25. Parzych, K. R. & Klionsky, D. J. An overview of autophagy: morphology, mechanism, and regulation. *Antioxid. Redox Signal.* **20**, 460–73 (2014).

26. Wen, X. & Klionsky, D. J. An overview of macroautophagy in yeast. *J. Mol. Biol.* **428**, 1681–99 (2016).

27. Eisenberg, T. *et al.* Induction of autophagy by spermidine promotes longevity. *Nat. Cell Biol.* **11**, 1305–1314 (2009).

28. Morselli, E. *et al.* Autophagy mediates pharmacological lifespan extension by spermidine and resveratrol. *Aging (Albany. NY).* **1**, 961–70 (2009).

29. Ghosh, A. K., Mau, T., O'Brien, M., Garg, S. & Yung, R. Impaired autophagy activity is linked to elevated ER-stress and inflammation in aging adipose tissue. *Aging (Albany. NY).* **8**, 2525–2537 (2016).

30. Tasset, I. & Cuervo, A. M. Role of chaperone-mediated autophagy in metabolism. *FEBS J.* **283**, 2403–13 (2016).

31. Moreno-Blas, D., Gorostieta-Salas, E. & Castro-Obregón, S. Connecting chaperone-

mediated autophagy dysfunction to cellular senescence. *Ageing Res. Rev.* **41**, 34–41 (2018).

32. Kaushik, S. & Cuervo, A. M. Chaperone-mediated autophagy: a unique way to enter the lysosome world. *Trends Cell Biol.* **22**, 407–417 (2012).

33. Cuervo, A. M. & Wong, E. Chaperone-mediated autophagy: roles in disease and aging. *Cell Res.* **24**, 92–104 (2014).

34. Xilouri, M. *et al.* Impairment of chaperone-mediated autophagy induces dopaminergic neurodegeneration in rats. *Autophagy* **12**, 2230–2247 (2016).

35. Salvador, N., Aguado, C., Horst, M. & Knecht, E. Import of a Cytosolic Protein into Lysosomes by Chaperone-Mediated Autophagy depends on its Folding State. *J. Biol. Chem.* **275**, 27447–56 (2000).

36. Cuervo, A. M. & Dice, J. F. Age-related decline in chaperone-mediated autophagy. *J. Biol. Chem.* **275**, 31505–13 (2000).

37. Kiffin, R. *et al.* Altered dynamics of the lysosomal receptor for chaperone-mediated autophagy with age. *J. Cell Sci.* **120**, 782–91 (2007).

38. Zhang, C. & Cuervo, A. M. Restoration of chaperone-mediated autophagy in aging liver improves cellular maintenance and hepatic function. *Nat. Med.* **14**, 959–65 (2008).

39. Edkins, A. L. CHIP: A Co-chaperone for Degradation by the Proteasome. in 219–242 (Springer, Cham, 2015). doi:10.1007/978-3-319-11731-7_11

40. Hartl, F. U., Bracher, A. & Hayer-Hartl, M. Molecular chaperones in protein folding and proteostasis. *Nature* **475**, 324–332 (2011).

41. Hartl, F. U. Molecular chaperones in cellular protein folding. *Nature* **381**, 571–580 (1996).

42. Hartl, F. U. & Hayer-Hartl, M. Converging concepts of protein folding in vitro and in vivo. *Nat. Struct. Mol. Biol.* **16**, 574–581 (2009).

43. Young, J. C. The role of the cytosolic HSP70 chaperone system in diseases caused by misfolding and aberrant trafficking of ion channels. *Dis. Model. Mech.* **7**, 319–329 (2014).

44. Goloubinoff, P. Editorial: The HSP70 Molecular Chaperone Machines. *Front. Mol. Biosci.* **4**, (2017).

45. Daugaard, M., Rohde, M. & Jäättelä, M. The heat shock protein 70 family: Highly homologous proteins with overlapping and distinct functions. *FEBS Lett.* **581**, 3702–3710 (2007).

46. Lopez, T., Dalton, K. & Frydman, J. The Mechanism and Function of Group II Chaperonins. *J. Mol. Biol.* **427**, 2919–30 (2015).

47. Frydman, J. Folding of Newly Translated Proteins In Vivo: The Role of Molecular Chaperones. *Annu. Rev. Biochem.* **70**, 603–647 (2001).

48. Gruber, R. & Horovitz, A. Allosteric Mechanisms in Chaperonin Machines. *Chem.*

Rev. **116**, 6588–6606 (2016).

49. Ditzel, L. *et al.* Crystal structure of the thermosome, the archaeal chaperonin and homolog of CCT. *Cell* **93**, 125–38 (1998).

50. Llorca, O. *et al.* Eukaryotic type II chaperonin CCT interacts with actin through specific subunits. *Nature* **402**, 693–696 (1999).

51. Tian, G., Vainberg, I. E., Tap, W. D., Lewis, S. A. & Cowan, N. J. Specificity in chaperonin-mediated protein folding. *Nature* **375**, 250–253 (1995).

52. Roh, S.-H., Kasembeli, M., Bakthavatsalam, D., Chiu, W. & Tweardy, D. J. Contribution of the Type II Chaperonin, TRiC/CCT, to Oncogenesis. *Int. J. Mol. Sci.* **16**, 26706–20 (2015).

53. Pearl, L. H. & Prodromou, C. Structure and Mechanism of the Hsp90 Molecular Chaperone Machinery. *Annu. Rev. Biochem.* **75**, 271–294 (2006).

54. Wang, Y. *et al.* HSP90: a promising broad-spectrum antiviral drug target. *Arch. Virol.* **162**, 3269–3282 (2017).

55. Taipale, M. *et al.* Quantitative analysis of HSP90-client interactions reveals principles of substrate recognition. *Cell* **150**, 987–1001 (2012).

56. de Toda, I. M. & De la Fuente, M. The role of Hsp70 in oxi-inflamm-aging and its use as a potential biomarker of lifespan. *Biogerontology* **16**, 709–721 (2015).

57. Kirstein, J. *et al.* In vivo properties of the disaggregase function of J-proteins and Hsc70 in Caenorhabditis elegans stress and aging. *Aging Cell* **16**, 1414–1424 (2017).

58. de Toda, I. M., Vida, C., Ortega, E. & De La Fuente, M. Hsp70 basal levels, a tissue marker of the rate of aging and longevity in mice. *Exp. Gerontol.* **84**, 21–28 (2016).

59. Kaushik, S. & Cuervo, A. M. Proteostasis and aging. *Nat. Med.* **21**, 1406–1415 (2015).

60. Walter, P. & Ron, D. The unfolded protein response: from stress pathway to homeostatic regulation. *Science* **334**, 1081–6 (2011).

61. Santos, C. X. C., Tanaka, L. Y., Wosniak, J. & Laurindo, F. R. M. Mechanisms and Implications of Reactive Oxygen Species Generation During the Unfolded Protein Response: Roles of Endoplasmic Reticulum Oxidoreductases, Mitochondrial Electron Transport, and NADPH Oxidase. *Antioxid. Redox Signal.* **11**, 2409–2427 (2009).

62. Badiola, N. *et al.* Induction of ER stress in response to oxygen-glucose deprivation of cortical cultures involves the activation of the PERK and IRE-1 pathways and of caspase-12. *Cell Death Dis.* **2**, e149 (2011).

63. Badr, C. E., Hewett, J. W., Breakefield, X. O. & Tannous, B. A. A highly sensitive assay for monitoring the secretory pathway and ER stress. *PLoS One* **2**, e571 (2007).

64. Szegezdi, E. *et al.* ER stress contributes to ischemia-induced cardiomyocyte apoptosis. *Biochem. Biophys. Res. Commun.* **349**, 1406–1411 (2006).

65. Urra, H., Dufey, E., Lisbona, F., Rojas-Rivera, D. & Hetz, C. When ER stress reaches a dead end. *Biochim. Biophys. Acta - Mol. Cell Res.* **1833**, 3507–3517 (2013).

66. Tabas, I. & Ron, D. Integrating the mechanisms of apoptosis induced by endoplasmic reticulum stress. *Nat. Cell Biol.* **13**, 184–90 (2011).

67. Schröder, M. & Kaufman, R. J. THE MAMMALIAN UNFOLDED PROTEIN RESPONSE. *Annu. Rev. Biochem.* **74**, 739–789 (2005).

68. Toth, A. *et al.* Endoplasmic Reticulum Stress as a Novel Therapeutic Target in Heart Diseases. *Cardiovasc. Hematol. Disord. Targets* **7**, 205–218 (2008).

69. Paz Gavilán, M. *et al.* Cellular environment facilitates protein accumulation in aged rat hippocampus. *Neurobiol. Aging* **27**, 973–982 (2006).

70. Paz GavilÃ¡n, M. *et al.* Dysfunction of the unfolded protein response increases neurodegeneration in aged rat hippocampus following proteasome inhibition. *Aging Cell* **8**, 654–665 (2009).

71. Chalil, S. *et al.* Increased Endoplasmic Reticulum Stress in Mouse Osteocytes with Aging Alters Cox-2 Response to Mechanical Stimuli. *Calcif. Tissue Int.* **96**, 123–128 (2015).

72. Armstrong, J. L., Flockhart, R., Veal, G. J., Lovat, P. E. & Redfern, C. P. F. Regulation of endoplasmic reticulum stress-induced cell death by ATF4 in neuroectodermal tumor cells. *J. Biol. Chem.* **285**, 6091–6100 (2010).

73. Bertolotti, A. *et al.* Increased sensitivity to dextran sodium sulfate colitis in IRE1beta-deficient mice. *J. Clin. Invest.* **107**, 585–93 (2001).

74. Chen, Y. & Brandizzi, F. IRE1: ER stress sensor and cell fate executor. *Trends in Cell Biology* **23**, 547–555 (2013).

75. Adams, C. J., Kopp, M. C., Larburu, N., Nowak, P. R. & Ali, M. M. U. Structure and molecular mechanism of ER stress signaling by the unfolded protein response signal activator IRE1. *Frontiers in Molecular Biosciences* **6**, (2019).

76. Wee, P. & Wang, Z. Epidermal growth factor receptor cell proliferation signaling pathways. *Cancers* **9**, (2017).

77. Conte, A. & Sigismund, S. Chapter Six - The Ubiquitin Network in the Control of EGFR Endocytosis and Signaling. *Prog. Mol. Biol. Transl. Sci.* **141**, 225–76 (2016).

78. Zou, J. *et al.* Mechanisms shaping the role of ERK1/2 in cellular senescence (Review). *Mol. Med. Rep.* **19**, 759–770 (2019).

79. Boucher, M.-J., Jean, D., Vézina, A. & Rivard, N. Dual role of MEK/ERK signaling in senescence and transformation of intestinal epithelial cells. *Am. J. Physiol. Gastrointest. Liver Physiol.* **286**, G736-46 (2004).

80. De Marco, M. *et al.* Role of BAG3 in cancer progression: A therapeutic opportunity. *Semin. Cell Dev. Biol.* **78**, 85–92 (2018).

81. Stürner, E. & Behl, C. The Role of the Multifunctional BAG3 Protein in Cellular Protein Quality Control and in Disease. *Front. Mol. Neurosci.* **10**, 177 (2017).

82. Minoia, M. *et al.* BAG3 induces the sequestration of proteasomal clients into cytoplasmic puncta. *Autophagy* **10**, 1603–1621 (2014).

83. Alberti, S., Esser, C. & Höhfeld, J. BAG-1--a nucleotide exchange factor of Hsc70 with multiple cellular functions. *Cell Stress Chaperones* **8**, 225–31 (2003).

84. Kovalevich, J. & Langford, D. Considerations for the use of SH-SY5Y neuroblastoma cells in neurobiology. *Methods Mol. Biol.* **1078**, 9–21 (2013).

85. Ross, R. A., Spengler, B. A. & Biedler, J. L. Coordinate morphological and biochemical interconversion of human neuroblastoma cells. *J. Natl. Cancer Inst.* **71**, 741–7 (1983).

86. Muhaisen, A. *et al.* Sequential treatment of SH-SY5Y cells with retinoic acid and brain-derived neurotrophic factor gives rise to fully differentiated, neurotrophic factor-dependent, human neuron-like cells. *J. Neurochem.* **75**, 991–1003 (2000).

87. Påhlman, S., Ruusala, A. I., Abrahamsson, L., Mattsson, M. E. & Esscher, T. Retinoic acid-induced differentiation of cultured human neuroblastoma cells: a comparison with phorbolester-induced differentiation. *Cell Differ.* **14**, 135–44 (1984).

88. Trypan Blue Staining Assay | Creative Bioarray. Available at: https://www.creative-bioarray.com/support/trypan-blue-staining-assay.htm. (Accessed: 18th September 2019)

89. Elliott, A. A practical guide to the study of calcium in living cells. *Cell Calcium* **16**, 347–348 (1994).

90. Guillemette, T. *et al.* Methods for Investigating the UPR in Filamentous Fungi. *Methods Enzymol.* **490**, 1–29 (2011).

91. Uppala, J. K., Gani, A. R. & Ramaiah, K. V. A. Chemical chaperone, TUDCA unlike PBA, mitigates protein aggregation efficiently and resists ER and non-ER stress induced HepG2 cell death. *Sci. Rep.* **7**, (2017).

92. Zhang, Y. *et al.* Tauroursodeoxycholic acid (TUDCA) alleviates endoplasmic reticulum stress of nuclear donor cells under serum starvation. *PLoS One* **13**, (2018).

93. Resazurin Cell Viability Assay | Creative Bioarray. Available at: https://www.creative-bioarray.com/support/resazurin-cell-viability-assay.htm. (Accessed: 18th September 2019)

94. Appropriate Fixation of IHC/ICC Samples: R&D Systems. Available at: https://www.rndsystems.com/resources/protocols/appropriate-fixation-ihcicc-samples. (Accessed: 25th September 2019)

95. Zampieri, S. *et al.* The use of Tween 20 in immunoblotting assays for the detection of autoantibodies in connective tissue diseases. *J. Immunol. Methods* **239**, 1–11 (2000).

96. Pierce™ BCA Protein Assay Kit. Available at: https://www.thermofisher.com/order/catalog/product/23225. (Accessed: 18th September 2019)

97. Bustin, S. A. & Mueller, R. Real-time reverse transcription PCR (qRT-PCR) and its potential use in clinical diagnosis. *Clin. Sci.* **109**, 365–379 (2005).

98. *NZYTaq 2× Green Master Mix, separate MgCl 2*.

99. Chemiluminescent Western Blotting - PT.

100. Kennedy, D., Samali, A. & Jäger, R. Methods for studying ER stress and UPR markers in human cells. *Methods Mol. Biol.* **1292**, 3–18 (2015).

101. Verwilst, P. *et al.* Revealing Protein Aggregates under Thapsigargin-Induced ER Stress Using an ER-Targeted Thioflavin. *ACS Sensors* acssensors.9b00568 (2019). doi:10.1021/acssensors.9b00568

102. Mlynarczyk, C. & Fåhraeus, R. Endoplasmic reticulum stress sensitizes cells to DNA damage-induced apoptosis through p53-dependent suppression of p21 CDKN1A. *Nat. Commun.* **5**, (2014).

103. Sehgal, P. *et al.* Inhibition of the sarco/endoplasmic reticulum (ER) Ca2-ATPase by thapsigargin analogs induces cell death via ER Ca2 depletion and the unfolded protein response. *J. Biol. Chem.* **292**, 19656–19673 (2017).

104. Panagaki, T., Michael, M. & Hölscher, C. Liraglutide restores chronic ER stress, autophagy impairments and apoptotic signalling in SH-SY5Y cells. *Sci. Rep.* **7**, (2017).

105. Huang, S. *et al.* Tunicamycin potentiates paclitaxel-induced apoptosis through inhibition of PI3K/AKT and MAPK pathways in breast cancer. *Cancer Chemother. Pharmacol.* **80**, 685–696 (2017).

106. Cortez, L. & Sim, V. The therapeutic potential of chemical chaperones in protein folding diseases. *Prion* **8**, 1–6 (2014).

107. Rodrigues, C. M., Fan, G., Wong, P. Y., Kren, B. T. & Steer, C. J. Ursodeoxycholic acid may inhibit deoxycholic acid-induced apoptosis by modulating mitochondrial transmembrane potential and reactive oxygen species production. *Mol. Med.* **4**, 165–78 (1998).

108. Azzaroli, F. Ursodeoxycholic acid diminishes Fas-ligand–induced apoptosis in mouse hepatocytes. *Hepatology* **36**, 49–54 (2002).

109. Rodrigues, C. M. P., Solá, S., Sharpe, J. C., Moura, J. J. G. & Steer, C. J. Tauroursodeoxycholic Acid Prevents Bax-Induced Membrane Perturbation and Cytochrome *c* Release in Isolated Mitochondria †. *Biochemistry* **42**, 3070–3080 (2003).

110. Hylemon, P. B. *et al.* Bile acids as regulatory molecules. *Journal of Lipid Research* **50**, 1509–1520 (2009).

111. Berger, E. & Haller, D. Structure-function analysis of the tertiary bile acid TUDCA for the resolution of endoplasmic reticulum stress in intestinal epithelial cells. *Biochem. Biophys. Res. Commun.* **409**, 610–615 (2011).

112. Lièvremont, J. P., Rizzuto, R., Hendershot, L. & Meldolesi, J. BiP, a major chaperone protein of the endoplasmic reticulum lumen, plays a direct and important

role in the storage of the rapidly exchanging pool of Ca2+. *J. Biol. Chem.* **272**, 30873–30879 (1997).

113. Hamdan, N., Kritsiligkou, P. & Grant, C. M. ER stress causes widespread protein aggregation and prion formation. *J. Cell Biol.* **216**, 2295–2304 (2017).

114. Sarcoplasmic Reticulum - an overview | ScienceDirect Topics. Available at: https://www.sciencedirect.com/topics/neuroscience/sarcoplasmic-reticulum. (Accessed: 12th November 2019)

115. Chen, J. C., Castillo, A. B. & Jacobs, C. R. Cellular and Molecular Mechanotransduction in Bone. in *Osteoporosis: Fourth Edition* 453–475 (Elsevier Inc., 2013). doi:10.1016/B978-0-12-415853-5.00020-0

116. Tripathi, A. & Chaube, S. K. High cytosolic free calcium level signals apoptosis through mitochondria-caspase mediated pathway in rat eggs cultured in vitro. *Apoptosis* **17**, 439–448 (2012).

117. Han, J. *et al.* ER-stress-induced transcriptional regulation increases protein synthesis leading to cell death. *Nat. Cell Biol.* **15**, 481–490 (2013).

118. Anderson, L. L., Mao, X., Scott, B. A. & Crowder, C. M. Survival from hypoxia in C. elegans by inactivation of aminoacyl-tRNA synthetases. *Science (80-.).* **323**, 630–633 (2009).

119. Yang, Y. *et al.* The ER-localized Ca2-binding protein calreticulin couples ER stress to autophagy by associating with microtubule-associated protein 1A/1B light chain 3. *J. Biol. Chem.* **294**, 772–782 (2019).

120. Guo, F. J. *et al.* ATF6 upregulates XBP1S and inhibits ER stress-mediated apoptosis in osteoarthritis cartilage. *Cell. Signal.* **26**, 332–342 (2014).

121. Li, G. *et al.* Role of ERO1-α-mediated stimulation of inositol 1,4,5-triphosphate receptor activity in endoplasmic reticulum stress-induced apoptosis. *J. Cell Biol.* **186**, 783–792 (2009).

122. Sano, R. & Reed, J. C. ER stress-induced cell death mechanisms. *Biochimica et Biophysica Acta - Molecular Cell Research* **1833**, 3460–3470 (2013).

123. Felzen, V. *et al.* Estrogen receptor α regulates non-canonical autophagy that provides stress resistance to neuroblastoma and breast cancer cells and involves BAG3 function. *Cell Death Dis.* **6**, (2015).

124. Yao, Y. *et al.* A non-canonical pathway regulates ER stress signaling and blocks ER stress-induced apoptosis and heart failure. *Nat. Commun.* **8**, (2017).

Appendix

Cell Culture solutions

PBS (1x)

For a final volume of 500 mL, one pack of BupH Modified Dulbecco's Phosphate Saline Pack (Pierce) is dissolves in deionised H_2O.

Final composition:

- 8 mM Sodium Phosphate (Na_2HPO_4)

- 2 mM Potassium Phosphate (KH_2PO_4)

- 140 mM Sodium Chloride (NaCl)

- 10 mM Potassium Chloride (KCl)

Sterilization is done by filtering through a 0,2µm filter and store at 4ºC.

Culture medium

Freezing Medium

SDS-PAGE and Western Blot solutions

LGB (lower gel buffer) (4x)

After adding 900 mL of deionised H_2O:

-Tris base ($C_4H_{11}NO_3$): 181.65 g (1,5 M)

- SDS ($NaC_{12}H_{25}SO_4$): 4 g (0,4%)

Mix until the solutes have dissolved. Adjust the pH to 8.9 and volume is adjusted to 1 L with deionised H_2O. Stored at 4ºC.

UGB (upper gel buffer) (5x)

After adding 900 mL of deionised H_2O:

- Tris base ($C_4H_{11}NO_3$): 75,69 g (0,5 M)

Mix until solute is dissolved. pH is adjusted to 6,8 and volume is adjusted with deionised H_2O until 1 L is achieved. Stored at 4ºC

10% APS (ammonium persulfate)

In 10 mL of deionised H_2O dissolve 1 g of APS. Store at 4ºC. Stable up to 1 week.

Note: Prepare fresh solution before using

10% SDS (sodium dodecyl sulfate)

In 10 mL of deionised H_2O dissolve 1 g of SDS.

1% SDS (sodium dodecyl sulfate)

In 9 mL of deionised H_2O dissolve 1 mL of 10% SDS solution.

1 M Tris (pH 6.8) solution

To 150 mL of deionised H_2O add:

- Tris base ($C_4H_{11}NO_3$): 30.3 g

Adjust the pH to 6,8 and adjust the final volume to 250 mL.

Loading Gel Buffer (4x)

- 1 M Tris solution (pH 6.8): 2.5 mL (250 mM)

- SDS ($NaC_{12}H_{25}SO_4$): 0,8 g (8%)

- Glycerol ($C_3H_8O_3$): 4 mL (40%)

- β-Mercaptoethanol ($C_2H_6O_3$): 2 mL (2%)

- Bromophenol blue ($C_{19}H_{10}Br_4O_5S$): 1 mg (0.01%)

Adjust the volume to 10 mL with deionised H_2O. Store at room temperature. Protect from light.

Resolving (lower) gel solution for gradient gels

Stacking (upper) gel solution

Running Buffer (10x)

Running Buffer (1x)

Transfer Buffer (10x)

To 900 mL of deionised H_2O add:

- Tris base ($C_4H_{11}NO_3$): 30.3 g (250 mM)

- Glycine ($C_2H_5NO_2$): 144.2 g (1.92 M)

Dissolve in deionised H_2O adjust the pH to 8.3 and adjust the volume to 1 L.

Transfer Buffer (1x)

Mix 100 mL of 10x Transfer Buffer, 200 mL of methanol and 700 mL of deionised H_2O.

Immunoblotting solutions

TBS (10x)

To 900 mL of deionised H_2O add:

- Tris base ($C_4H_{11}NO_3$): 12.11 g (10 mM)

- Sodium Chloride (NaCl): 87.66 g (150 mM)

Adjust the pH to 8.0 with HCl and adjust the volume to 1 L with deionised H_2O

TBS (1x)

In 900 mL of deionised H_2O dissolve 100 mL of 10x TBS solution.

TBS-T (10x) (TBS+Tween)

-Tris base ($C_4H_{11}NO_3$): 12,11 g (10 mM)

- Sodium Chloride (NaCl): 87,66 g (150 mM)

- Tween 20: 5 mL (0,05%)

Adjust the pH to 8,0 with HCl and adjust the volume to 1 L with deionised H_2O.

TBS-T (1x)

In 900 mL of deionised H_2O dissolve 100 mL of 10x TBS-T solution.

Immunocytochemistry solutions

4% Formaldehyde

For a final volume of 100 mL, add 4 g of paraformaldehyde to 25 mL deionised H_2O.

Dissolve by heating the mixture at 58ºC while stirring.

Add 1-2 drops of 1 M NaOH to clarify the solution and filter (0.2 µm filter).

Add 50 mL of 2x PBS and adjust the volume to 100 mL with deionised H_2O-

PBS-T (0,1% Tween)

Dissolve 100 µL of Triton X-100 in 100 mL of 1x PBS.

Cut the end of blue tip before aspirating Tween 20.

Stir for a long time with tip inside the bottle.

0.2% Triton X-100

Dissolve 200 µL of Triton X-100 in 100 mL of 1x PBS.

Cut the end of a blue tip before aspirating Triton X-100.

Stir for a long time with the tip inside the bottle.